DEVELOPMENT OF DIODE LASERS
FOR ULTRASHORT PULSE GENERATION

DEVELOPMENT OF InGaAsP/GaAs DIODE LASERS FOR ULTRASHORT PULSE GENERATION

by

JAMES ROSCOE, B. SC.

A Thesis
Submitted to the School of Graduate Studies
in partial fulfillment of the requirements
for the degree of
Master of Engineering

McMaster University

© Copyright by James R.Roscoe, March 1999.

MASTER OF ENGINEERING (1999)
(Engineering Physics)

McMaster University
Hamilton, Ontario

TITLE: Development of InGaAsP/GaAs Diode Lasers for Ultrashort Pulse Generation

AUTHOR: James R. Roscoe

SUPERVISORS: Dr. Harold Haugen and Dr. Peter Mascher

NUMBER OF PAGES: xi, 120

Abstract

The groundwork has been completed for a large new research initiative involving the development of diode lasers for moderate power ultrashort pulse generation. This thesis reports on the status of three core areas of this initiative: InGaAsP/GaAs diode laser design and characterization, split contact device testing, and thin film interference filter deposition and characterization.

Two new short wavelength diode laser designs have been realized and tested. A 980 nm laser was designed, using an InGaAsP barrier/waveguide region. This showed improved far field performance and better contact isolation as compared to an existing 980 nm laser using GaAs barriers. A laser emitting at 850 nm was also designed using GaAs quantum wells surrounded by a new quaternary waveguide region.

A test arrangement was developed to facilitate the measurement of IV and LI curves for split contact lasers. Numerous lasers were tested, indicating that short absorber sections and narrow gap widths are preferable for use as saturable absorbing regions in a passively mode locked diode laser.

Finally, thin film silicon oxynitride interference filters have been designed, deposited, and characterized for several antireflecting and high reflectance coatings on semiconductor laser facets. A comparison of single layer AR coatings accounting for the modal reflectivity was performed. A four layer high reflectance coating with a peak broadband reflectance of over 90% was deposited on a laser facet.

Acknowledgments

I would like to thank Dr. Harold Haugen and Dr. Peter Mascher for their insight and direction in the supervision of this project. I would especially like to thank Steve Wallace for his invaluable contributions to many scientific aspects of this work. In particular, Steve performed the laser processing, developed the laser modeling code, and provided extensive assistance in the laser development, SEM, and thin film depositions reported in this thesis. Steve was also very helpful in the proofreading stages of this thesis as well as for many bits of general wisdom. I would like to thank Richard Wood for the code and electronics he developed during the two summers he worked with our research group. Thanks to Marcel Boudreau for his work on the CVD system and the code responsible for the calculations of modal reflectivity presented in this thesis. I would also like to acknowledge the other members of the group for their contributions to aspects of the bigger project not directly related to this thesis.

I would like to acknowledge the MBE group for their contributions to this project. Many thanks to Brad Robinson for his efforts in the MBE growth of the laser structures studied in this thesis. Additionally, thanks are extended to Dr. David Thompson for providing the original SQW 980 nm lasers described in this thesis.

Table of Contents

1 Introduction **1**

1.1 Motivation 1

1.2 Project Objectives 3

2 An Overview of Ultrafast Diode Laser Theory **5**

2.1 The Basics 5

2.2 Active Mode Locking 7

2.3 Passive Mode Locking 9

2.4 Hybrid Mode Locking 15

2.5 Gain Switching 16

2.6 Time/Bandwidth, Chirp, and Pulse Compression 17

3 Design and Characterization of Lasers for Mode Locking **19**

3.1 Design Goals 19

3.1.1 Wavelength 19

3.1.2 Efficiency and Threshold 21

3.1.3 Beam Properties 22

3.1.4 High Power 23

3.1.5 Modulation Bandwidth 24

3.2 Laser Modeling and Design 25

3.2.1 The Model 26

3.2.2 Active Region Design 33

3.2.4 Quaternary Interpolations 35

3.3 Measurement Apparatus 37

3.4 980 nm Lasers 38

3.5 850 nm Lasers 46

3.6 Future Laser Designs 52

4 Split Contact Theory and Characterization 57

4.1 Split Contact Biasing Theory 57

4.2 The Effects of Biasing on Temporal Characteristics 62

4.3 Experimental Design for Multisegment IV Characterization 63

4.4 Results from Split Contact Characterization 65

5 Antireflection Coatings 71

5.1 Thin Film Deposition using ECR-CVD 72

5.2 Antireflection Coating Design 77

5.3 Characterization of AR Coatings 83

5.4 Characterization of Modal Reflectivity 85

5.5 Single Layer AR Coatings on Laser Facets 87

5.6 High Reflectance Coatings 93

6 Conclusions 99

6.1 Laser Designs 100

6.2 Split Contact Design and Characterization 102

6.3 Thin Film Interference Coatings 104

6.4 Future Work 105

References **109**

List of Figures

2.1 Effect of increasing the number of modes locked in phase (2, 4, and 10) for a 30 cm cavity 6

3.1 Effective index technique for a rectangular dielectric waveguide 26

3.2 Ridge waveguide structure 27

3.3 Simplified ridge waveguide structure for the model 28

3.4 The effective index method, applied to a ridge waveguide 29

3.5 Coordinate system used in the far field calculation 31

3.6 Quantum well energy levels 34

3.7 Diode laser test configuration 38

3.8 The band structure of the existing 980 nm laser design 39

3.9 The band structure for 980 nm lasers from growth #2391. The quaternary had an approximate composition of x=0.585 and y=0.140 ($In_{1-x}Ga_xAs_yP_{1-y}$) . . . 41

3.10 Ridge of a 980 nm laser 42

3.11 Feature perpendicular to ridge 42

3.12 Typical LI curves for several ridge widths of lasers from growth 2391 43

3.13 A damaged ridge 44

3.14 Ridge damage near facet 44

3.15 Optical spectra of a 980 nm laser . . . 45

3.16 The band structure for 850 nm lasers from growth 2486. The quaternary had an approximate composition of x=0.766 and y=0.510 ($In_{1-x}Ga_xAs_yP_{1-y}$) . . . 47

3.17 The ridge of an 850 nm laser diode . . . 47

3.18 A typical LI curve for lasers from growth 2486 . . . 48

3.19 Optical spectra of an 850 nm laser . . . 49

3.20 An 850 nm laser above threshold (53 mA) . . . 50

4.1 Electrical connection to a split contact laser . . . 58

4.2 Simulated split contact IV curves for different gain section currents . . . 59

4.3 Programmable voltage source for absorber section biasing . . . 65

4.4 Geometry of the split contact lasers tested (all dimensions in μm) . . . 66

4.5 Split contact IV curves for varying gain section biases for four lasers with different gap widths . . . 68

4.6 Split contact IV curves for varying gain section biases for four lasers with different gain section / absorber section ratios . . . 70

5.1 The McMaster ECR-CVD system . . . 73

5.2 The silicon precursors . . . 75

5.3 Mounting a laser bar for a deposition . . . 76

5.4 Comparison of single layer and two layer AR designs for 980 nm on a substrate with n=3.6 . . . 78

5.5 Comparison of AR designs for the existing SQW 980 nm laser design (988 nm) . 81

5.6 Comparison of AR designs for lasers processed from growth 2391 (994 nm) . . 81

5.7 Comparison of AR designs for lasers processed from growth 2486 (850 nm) . . 82

5.8 Estimation of uncertainty introduced into the film reflectivity profile due to deposition system tolerances 83

5.9 Reflectivity profile for the AR coating accounting for modal reflectivity as deposited on the silicon witness sample 89

5.10 Reflectivity profile for the AR coating based on the plane wave model as deposited on a silicon witness sample 89

5.11 Comparison of spectra before and after coating laser 10b with the modal reflectivity AR design 90

5.12 Comparison of average RG products before and after AR coating laser 12b with the film accounting for modal reflectivity 91

5.13 Comparison of average RG products before and after AR coating laser 9b with the plane wave filter 92

5.14 The reflectance profile of a four layer high reflectance stack deposited on an InP witness sample 95

6.1 Two possible external cavity configurations 106

List of Tables

5.1 Specification of AR coating parameters for the plane wave and modal designs given for each laser 82

5.2 Specification of a four layer HR stack for 980 nm 95

Chapter 1: Introduction

1.1 Motivation

In recent years, "ultrafast" laser technology has evolved to a point where commercial applications are becoming increasingly realizable. Historically, lasers capable of emitting very short, moderate power pulses have been sophisticated dye, excimer, or solid state crystal laser systems. In particular, the development of the Ti:sapphire laser in the early 1990's has revolutionized the ultrafast laser world. These lasers are capable of achieving pulse widths on the order of 5 to 10 fs with amplified peak powers in the terawatt regime [1, 2]. However, Ti:sapphire lasers are bulky and sophisticated to build, since they require substantial pump sources and a large optical cavity. Although the development of diode pumped solid state pump sources has reduced the size requirements somewhat, there is still a demand to produce ultrafast lasers in a more commercially accessible form for use in industrial applications.

Concurrently, the development of improved diode lasers has led to many inexpensive solutions in many laser applications. A particularly relevant example of this are the high power diode laser arrays that are now frequently used to pump solid state laser systems [3]. Diode lasers are inherently more compact and efficient than other pump sources used, thereby reducing the cost to manufacture the laser and to operate it.

While diode pumping of solid state systems reduces the size and cost of the laser, further improvements could be made in these areas by eliminating many of the "macroscopic" optical components entirely. This may be achievable in many applications by designing a diode laser capable of generating moderately powerful ultrafast pulses. Thus it is of scientific and commercial interest to contribute to the development of high power ultrafast diode lasers.

Fortunately, many properties of diode lasers make them quite well suited to the generation of ultrashort optical pulses. In particular, diode lasers typically have a wide gain bandwidth, can be directly electrically modulated with a wide bandwidth signal, and can be biased to operate as saturable absorbers. These properties allow diode lasers to be mode locked actively, passively, or by combining active and passive techniques.

Research investigating ultrashort pulse generation by diode lasers has been pursued for a number of years. The earliest observations of ultrashort pulses from diode lasers were made in the late 1960's [4]. However, the most interesting developments have occurred over the past two decades, since the first demonstration of active mode locking of an external cavity diode laser in 1978 [5]. Current mode locked diode laser technology is capable of producing pulses in the 1 ps regime [6, 7, 8]. By combining this with amplification and chirp compensation, pulses as short as 200 fs with peak powers as high as 160 W have been obtained [9, 10, 11].

1.2 Project Objectives

The objective of the overall group project is to develop diode laser sources capable of producing ultrashort pulses with moderately high peak powers. Such lasers would be suitable for many applications including those requiring multiphoton interactions. In the short term, development of lasers suitable for hybrid mode locking and infrastructure suitable for driving and measuring such lasers is of the greatest importance. As the project matures, it would be of interest to study such areas as semiconductor laser amplifiers and pulse compression schemes. This would make it possible to achieve shorter pulses with higher peak powers than is realizable with a simple mode locked diode laser.

These objectives necessitate parallel studies of a number of different aspects that will be part of the final design. These include the development of multisegment diode lasers and amplifiers, thin film interference filter coating of laser facets, external cavity design, pulse compression design, and RF pulse generator design. Characterization of the performance of each of these aspects is critical to the final goals.

This is a new project which will be affiliated with the ultrafast laser research initiatives currently under development. The ultrafast laser facility will connect many different research groups and involve a substantial amount of equipment and personnel. The present system involves an amplified ultrafast Ti:sapphire based laser system. This may be used to conduct experiments investigating properties of the semiconductor

material relevant to mode locking diode lasers. In addition, the larger system may be used to characterize the needs of applications for which diode laser sources might be suitable in the future.

There are three sub-areas of the project that have been investigated in parallel to compose this thesis. Each of these areas is considered as a separate chapter. They are preceded by chapter 2 which outlines the basic theory necessary to understand the design goals discussed throughout the thesis. Chapter 3 covers the design, development, and characterization of short wavelength diode lasers suitable for mode locking applications. In chapter 4, the characterization of split contact devices will be discussed making connections to considerations for optimal passive mode locking of a laser. Chapter 5 will present results of the development and characterization of thin film coatings for diode laser facets, again making reference to the requirements to mode lock an external cavity diode laser. Finally, conclusions regarding the current state of the larger project will be drawn, including a reiteration of the important accomplishments to date and suggestions for future research.

Chapter 2: An Overview of Ultrafast Diode Laser Theory

2.1 The Basics

There are three approaches to generate ultrashort pulses using semiconductor lasers, i.e., gain switching, Q-switching, and mode locking. Of these, the most interesting process in terms of generating the shortest, highest power pulses is mode locking. Hence this thesis will concentrate on the development of lasers for mode locking.

A laser is said to be mode locked when it is driven such that it lases on several longitudinal modes simultaneously and when a number of these modes are locked in phase with one another. The temporal superposition of the in-phase waves results in high energy pulses repeated at a period defined by the cavity round trip time (2L/c). A generalized mathematical expression for this is the sum of the m contributing modes,

$$I(t) = \sum_m I_m \sin\left(\omega t + \frac{m\pi c}{L} t + \phi_m\right) \tag{2.1}$$

where the phase difference between modes ($\phi_m - \phi_{m-1}$) is constant. Because the pulses are generated due to the superposition of the waves from each mode, if many modes contribute to the output, the pulses are of very high intensity. Figure 2.1 demonstrates the effect of increasing the number of locked modes on the envelope of the optical intensity of a mode locked laser.

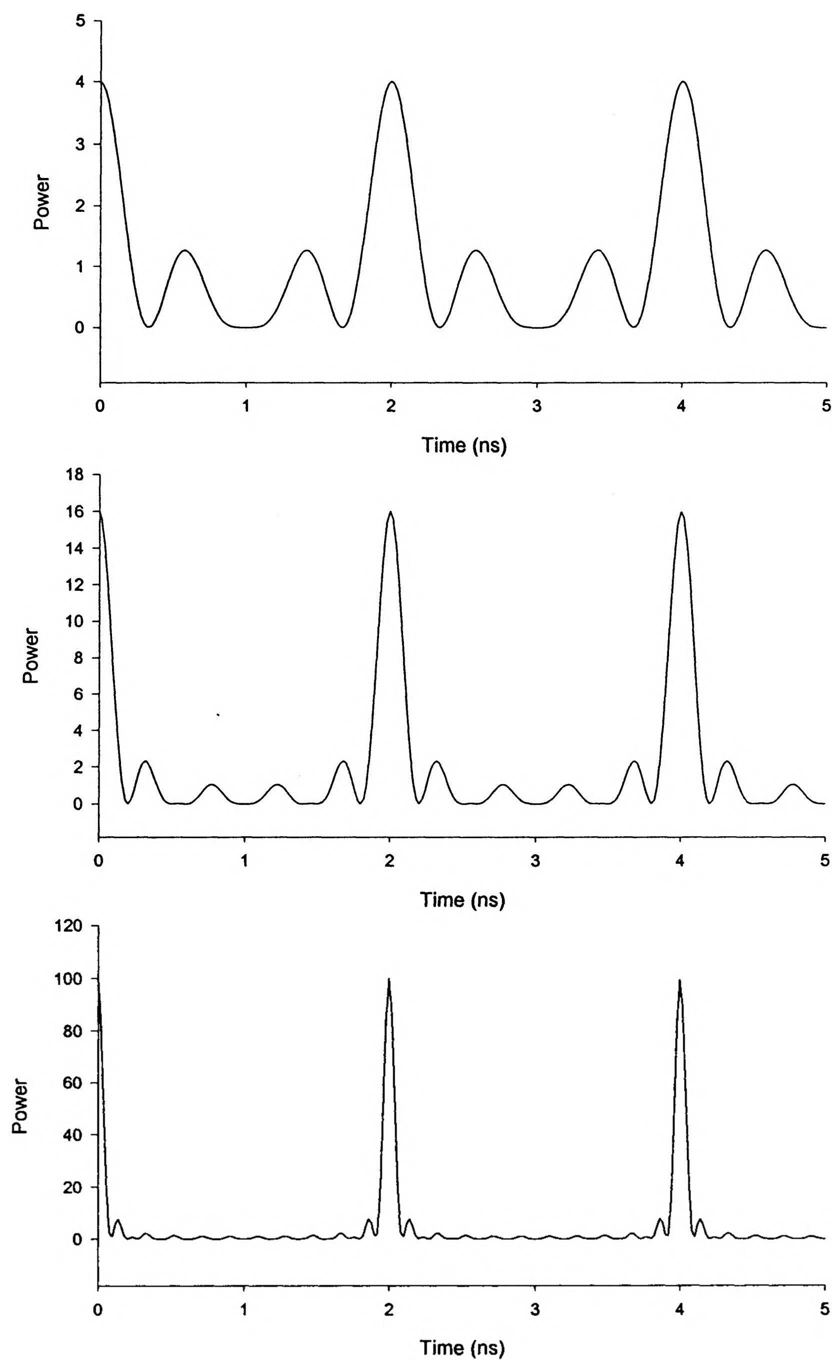

Figure 2.1: Effect of increasing the number of modes locked in phase (2, 4, and 10) for a 30 cm cavity. Note the change of scale on the vertical axis.

A laser can be mode locked using either "active" or "passive" methods. The underlying theory for each is somewhat different, and each has different attributes when considered in the context of diode lasers. These two methods are often implemented simultaneously in diode lasers with superior results in what is termed a hybrid mode locking scheme. The following sections will describe these three mode locking approaches within the context of diode lasers.

2.2 Active Mode Locking

Active mode locking, as the name suggests, involves driving the laser with an electrical signal that can be externally controlled. This electrical signal must be chosen such that the laser output meets the criteria for mode locking. Although there are several ways to achieve this, throughout this thesis, all references to active mode locking will refer to the most common method of mode locking diode lasers, that being AM (amplitude modulation) mode locking. A good description of FM (frequency modulation) mode locking, as applied to diode lasers is given by Nagar et al. [12].

AM mode locking is achieved by driving the laser with a sinusoidal electrical input. If one considers the optical field with a time varying intensity (determined by the electrical input with frequency ω_{RF}),

$$E = E_o \cos(\omega_{RF} t) \cos(\omega t + \phi) \tag{2.2}$$

it is easy to show that frequency sidebands are generated of the form:

$$E = \frac{E_o}{2}\left[\cos(\omega t + \omega_{RF} t + \phi) + \cos(\omega t - \omega_{RF} t + \phi)\right] \tag{2.3}$$

When the driving frequency is tuned to coincide with the reciprocal of the cavity round trip time, the sidebands of each mode interact with the adjacent modes linking them in phase. This satisfies the conditions for mode locking (2.1).

In a solitary diode laser, the cavity round trip time is very short because the laser cavity itself is very short. As a result, such lasers must be driven with electrical signals at microwave frequencies (many tens to hundreds of GHz). This presents somewhat of a technical challenge, since it is not trivial to build a microwave source capable of driving diode lasers at such high frequencies.

Often, the most practical way to actively mode lock a semiconductor laser is to mount it in an external cavity. This increases the round trip time by increasing the cavity length. The pulse repetition frequency is also reduced because it is intrinsically tied to the cavity length through the definition of mode locking (2.1). This means that within certain constraints, the pulse repetition frequency may be chosen to suit the application by picking an appropriate cavity length.

In order to obtain short single pulses from a diode laser mounted in an external cavity, it is critical that the residual reflectivity of the facet through which feedback takes place is maintained below 10^{-4} [13, 14, 15]. If there is significant reflectivity at this facet, a coupled cavity will form, where the pulse obtains some feedback from the shorter cavity. Experimentally, this results in multiple spikes corresponding to the short cavity superimposed on each of the pulses separated by the external cavity round trip time. The details of antireflection coating design will be discussed in chapter 5.

2.3 Passive Mode Locking

Passive mode locking is achieved by introducing a saturable absorber into the laser cavity. This saturable absorber absorbs photons, creating a loss in the laser cavity, until all the states of the absorber are in their upper level. At this point, the absorber can no longer absorb photons, so it is said to be "saturated". This transition from absorbing to transparency results in an abrupt reduction in the cavity loss. Since the gain is then much higher than the loss, the laser lases, dumping photons until the gain drops to equal the loss and the absorber starts to absorb strongly once again, terminating the pulse. If the absorber recovery time is significantly shorter than the cavity round trip time, then the absorber will follow the beat frequency term of the interfering modes. This tends to link the modes in phase, as described mathematically by (2.1).

In order for the process described above to work, it is necessary for the absorber to saturate more easily than the gain. If the gain saturated faster than the absorber, then a steady state condition would be reached where the gain saturated, but there was a balance between the gain and loss such that the laser operates CW. Thus a suitable saturable absorber must be chosen. Fortunately, the absorbing properties of semiconductors can be optimized to realize an acceptable saturable absorber. There are several approaches that each take advantage of the attributes of different types of transitions possible in semiconductors. These are band to band transitions, transitions at nonradiative recombination centers, and excitons. Some background information related to these

mechanisms is necessary for a full appreciation of the various passive mode locking techniques.

Band to band transitions are usually the dominant mechanism of photon absorption and emission in semiconductors. These transitions are exploited to achieve gain in a laser where a state of dynamic "equilibrium" between stimulated absorption and emission is achieved for a given pump level. As the current injected into the laser is increased, the quasi-Fermi levels in the active region spread apart. The condition for net gain on a transition (of energy E_{21}) is that the quasi-Fermi levels separate beyond the transition energy (E_{Fc}-E_{Fv}>E_{21}). At this point the stimulated emission rate exceeds the stimulated absorption rate. As pumping is further increased the quasi-Fermi levels separate further. Under these conditions, photons of energy less than E_{Fc}-E_{Fv} experience net gain, while photons of energy greater than E_{Fc}-E_{Fv} are absorbed. In quantum well lasers, the presence of quantized energy levels produces steps in the gain/absorption profile as the photon energy is increased [16].

In a semiconductor band to band transition, the saturation energy is defined as

$$E_{sat} = \frac{h\nu A}{\partial g / \partial N}, \tag{2.4}$$

where hν is the energy of the photons, A is the cross-sectional area of the waveguide mode, and ∂g/∂N is the differential gain [6]. This saturation energy is the energy at which the gain or absorption saturates. Thus, for two regions of fixed waveguide cross-section but different gain, the saturation energy is inversely proportional to ∂g/∂N.

Defining the region of lower gain as the absorber section and the other as the gain section, then if we want $E_{sat}|_{abs} < E_{sat}|_{gain}$, then it is necessary that $\partial g/\partial N|_{abs} > \partial g/\partial N|_{gain}$.

Fortunately the differential gain in a semiconductor does have a sublinear dependence on carrier density. The material gain as a function of carrier density is reliably modeled using a three parameter fit as given in Coldren and Corzine [16]:

$$g = g_0 \ln\left(\frac{N + N_s}{N_{tr} + N_s}\right) \tag{2.5}$$

where N_{tr} is the transparency carrier density, N_s is the "shift" carrier density (used to ensure the logarithm is finite when N=0), and g_0 is an empirical gain coefficient. The differential gain as a function of carrier density is then just

$$\frac{\partial g}{\partial N} = \frac{g_0}{N + N_s}. \tag{2.6}$$

So, at the higher pumping rates required for increased gain, the denominator gets large causing $\partial g/\partial N$ to drop. Conversely, at low pumping rates where there is net absorption, the denominator is small and $\partial g/\partial N$ is large. Thus, $\partial g/\partial N|_{abs} > \partial g/\partial N|_{gain}$ and the absorption saturates more easily than the gain.

Although band to band transitions are most relevant for pumped semiconductors, at low carrier densities, the absorption peaks due to exciton absorption become dominant. These are particularly strong in reduced dimensional structures (such as quantum wells) as compared to bulk material. This is because the localization of carriers provided by the quantum structures increases the probability that an exciton will form. The result is numerous narrow peaks clustered around the band or sub-band edges [16]. Excitons are

particularly relevant to consider because their absorption peaks saturate at as much as ten times lower intensity than the direct band transitions [17]. This property can be exploited in order to make a good saturable absorber.

Early observation of unstable pulse trains generated by aging diode lasers lead to the discovery that absorption caused by defects in the semiconductor active region could be saturated suitably to achieve passive mode locking [18]. In order to gain better control over the introduction of defects in the laser, proton bombardment has been used to generate saturable absorption at one laser facet. The extent of the damage induced in the laser can be controlled by adjusting the proton energy and exposure time. Devices that have been processed in this way have been used in passive and hybrid mode locked devices [19].

The saturable absorption evident in these lasers results largely from the band to band absorption described previously. The presence of defects in the active region of these lasers can result in energy levels within the band gap. These nonradiative recombination centers, or traps, allow a net recombination rate that robs population from the upper state and hence the lasing transition. If the distribution of defects is non-uniform, then there can be localized regions of net absorption leading to the effects observed experimentally. Because nonradiative recombination centers tend to be fast at removing carriers in the absorbing regions, they tend to improve the absorber recovery time. This characteristic is very important since the spontaneous emission lifetime of

semiconductors (typically 1 ns) is too long to be an effective means of carrier removal for absorber recovery in mode locking [6].

Another way to implement saturable absorbers suitable for use with external cavity diode lasers is to fabricate multiquantum well mirrors. In order to enhance the absorber recovery time by increasing the carrier recombination rate, the beam must be tightly focused on the MQW mirror surface [7], or the mirrors must be proton bombarded [10]. This is preferable to inducing point defects in the actual laser active region since the MQW mirror is not electrically pumped, and hence it should not deteriorate with use (unlike the damaged lasers). Because they are not electrically pumped, saturable absorbers using MQW mirrors typically are designed to take advantage of exciton absorption at the laser wavelength. The primary drawback of MQW mirrors from a commercial standpoint is that they may not be practical for economical large scale production. This is because fabrication of the mirror involves relatively sophisticated processing that is usually reserved for the fabrication of thousands of devices.

A particularly convenient way of achieving saturable absorption in diode lasers is to fabricate multisection devices such that one section is biased for gain and another for absorption. These devices rely exclusively on the absorption characteristics of band to band transitions under different electrical biases as described earlier. The advantage of this is that many of the saturable absorber properties can then be controlled electrically, allowing device operation to be optimized after fabrication. The amount of absorption

can be controlled by changing the length of the absorbing section and adjusting the electrical biasing. The recovery time of the absorber can be shortened by applying a reverse bias to sweep out carriers [6].

Multisection diode lasers have been successfully mode locked using passive and hybrid techniques as monolithic devices as well as in external cavities [6]. Multiple contact lasers are commercially relevant because they cost little more to produce than single contact lasers. The difference simply amounts to the choice of masks used in the processing stages. Because of the many advantages of using split contact saturable absorbers, this was the methodology chosen for the devices used in this thesis. More detailed theory regarding the optimization of split contact geometries will be considered in chapter 4.

A variation on passive mode locking that results in shorter pulses is referred to as "colliding pulse" mode locking. This is achieved by placing the saturable absorber in the cavity such that counterpropagating pulses in the cavity overlap in the saturable absorber. The primary benefit of this is that in order for the counterpropagating pulses to "collide" in the absorber, they must pass through the gain section at different times. This makes it easier to saturate the absorber without saturating the gain since the peak intensity reached in the absorber is higher than in the gain section [6, 4].

2.4 Hybrid Mode Locking

Each of the previous methods of mode locking a diode laser has its drawbacks. Although the occurrence of multiple pulses in actively mode locked diode lasers can be reduced by suitable antireflection coatings, the satellite pulses tend to be very difficult to eliminate entirely. However, by introducing a saturable absorber with a fast recovery time (significantly less than the cavity round trip time), the weak secondary pulses will not be able to saturate the recovered absorber and will be attenuated [20].

At the same time, experimentally observed pulses from passively mode locked devices tend to be highly influenced by timing jitter since the pulse originates from the spontaneous emission in the cavity [4]. In contrast, jitter in actively mode locked diode lasers primarily results from jitter and amplitude noise in the RF oscillator [21]. Since this can be minimized by good oscillator design, active mode locking is considered to be preferable in timing sensitive applications.

The most successful mode locked diode laser designs combine the timing stability of active mode locking with the pulse shortening mechanisms of passive mode locking. A stable RF source can effectively seed the passive processes, reducing jitter while ensuring that a clean single pulse output is obtained. This combination of active and passive mechanisms is referred to as hybrid mode locking. Hybrid mode locked lasers have been implemented using ion bombarded lasers [22, 23] as well as multisection devices [6, 24]. Because of the demonstrated success of this approach, it is the target for our long term mode locked diode laser design.

2.5 Gain Switching

Although mode locking is of greatest importance to obtaining the shortest pulses with the highest power, there are some applications where a high pulse repetition rate is not desirable. Unfortunately, mode locking imposes the restriction that the pulse repetition rate is proportional to the reciprocal of the cavity round trip time. This means that if very short pulses are required at a lower repetition rate, a very large cavity would be required. To some extent, this defeats one of the primary benefits of using a diode laser: compactness.

A solution to this problem is to gain switch the lasers. In this case the laser is modulated with an ultrashort electrical pulse to switch the gain on and off. This creates a short optical pulse of moderate intensity where ideally the electrical pulse shuts off at the end of the laser's first relaxation oscillation. The difference between this and AM mode locking is that the gain switched electrical pulses can be arbitrarily spaced in time because adjacent modes do not need to be locked in phase. Thus a gain switched diode laser can operate at very low frequencies (hundreds of megahertz and below) without an external cavity. The drawback to this technique is that because the longitudinal modes are not locked in phase, less optical power can be obtained from a given pulse.

Any lasers developed to be suitable for active mode locking will also have suitable characteristics for gain switching at similar modulation speeds, and hence the lasers could be used for either as the application demands. Additionally, it is possible to

design RF oscillators that are suitable for both techniques, thus allowing the pulse characteristics to be compared.

2.6 Time/Bandwidth, Chirp, and Pulse Compression

To complete this chapter, it is worthwhile to take note of some fundamental issues that limit the pulse width achievable in diode lasers. It is a basic physical law that short pulses in time require a wide spectral bandwidth, as defined by the Fourier transform. This can be represented by,

$$\Delta \nu_{\min} \cong 1/\Delta t \tag{2.7}$$

where $\Delta\nu_{min}$ is the minimum spectral bandwidth for a pulse of duration Δt [13]. However, a pulse of width Δt can have a frequency content wider than $\Delta\nu_{min}$. This is frequently the case for ultrashort pulses generated in diode lasers. As a result, the pulse quality is often characterized by the time-bandwidth product $\Delta\nu\Delta t$.

The source of the excess bandwidth in pulses generated by diode lasers is a result of chirp. Chirp is defined as the change in frequency of the pulse as it evolves in time. Chirp in diode lasers can be traced back to the underlying theory of laser operation under pulsed conditions. As a mode locked pulse evolves towards its peak power, large variations in carrier density can occur. In diode lasers, the index of refraction of the active region is inherently a function of the carrier density. Thus the index of refraction changes as the pulse evolves. Since the wavelength is related to the index of refraction

such that $n_1\lambda_1=n_2\lambda_2$, the wavelength of the pulse inversely follows the index of refraction, leading to a pulse that changes wavelength as it evolves in time.

Because a chirped pulse changes frequency as a function of time, it is reasonable to expect that it would be possible to introduce an opposing chirp to compensate for the original chirp. By aligning the different frequency components of the pulse in time, the pulse would be shortened. This can be achieved by building a pulse compressor; a device which has different path lengths, and hence different propagation times, for different frequencies.

Frequency dependent propagation times implies dispersion, so compressors simply use linear dispersion to compensate the linear component of the chirp. This is easily accomplished by introducing an appropriately positioned diffraction grating pair [25]. The gratings are frequently placed in a telescope arrangement for adjustment of the amount and sign of the chirp [4, 26]. A very elegant way to provide chirp compensation is to use chirped optical fiber gratings [27, 28]. Another approach is to make use of appropriately chosen lengths of optical fiber to obtain sufficient compensating dispersion [29]. Due to the complicated relationship expressing carrier density evolution with the formation of the optical pulse, the chirp in diode lasers is not purely linear. These nonlinear components of the chirp can be removed by implementing higher order pulse compressors [10].

Chapter 3: Design and Characterization of Lasers for Mode Locking

3.1 Design Goals

The first step in the laser design process is to specify the target properties of the laser so that appropriate choices of design parameters can be made to meet these goals. There are tradeoffs among a number of the design goals so some care is necessary in choosing parameters that will result in a functional laser design.

3.1.1 Wavelength

The choice of wavelength is of primary importance because it restricts the choice of material systems that are suitable for the laser design. This is simply because the emission wavelength is related to the energy of the transition that generates the photon by

$$E=h\nu=hc/\lambda. \tag{3.1}$$

In a quantum well laser, the transition takes place in the quantum well with a transition energy slightly larger than the band gap of the material out of which the quantum well is made. In order to make a potential well using this material, it is necessary that it be surrounded by a material with a larger bandgap, known as the barrier. Additionally, the barrier material must also be surrounded by a larger band gap to provide optical waveguiding (this will be discussed further in section 3.2). In addition, all of the layers in a laser must be of similar lattice constant to ensure the laser has good crystal properties.

Thus there is a limited range of materials that satisfy all of the above conditions while producing a laser that emits within a certain wavelength range.

Although a wide range of wavelengths could be used to study the mode locking of diode lasers, short wavelength devices (less than 1 μm) are of the greatest interest to us for applications involving two photon absorption. Electronic transition energies are typically greater than 2 eV to 3 eV, or about 600 nm to 400 nm. Thus, a two photon transition would require photons with wavelengths shorter than about 1.2 μm to 800 nm. This wavelength range overlaps well with other facilities being developed as part of the more general ultrafast laser initiative, including a Ti:sapphire laser operating in the 750 nm to 850 nm regime. Compatibility with this equipment will allow other interesting studies to be performed in the future. Additionally, many other ultrafast diode laser research initiatives have focused primarily on the "telecommunications wavelengths" of 1.3 μm and 1.55 μm, so short wavelength research is of particular scientific interest.

Historically, lasers operating at wavelengths shorter than about 980 nm have been fabricated using the AlGaAs/GaAs ternary system to achieve the large bandgap required to produce short wavelength light. Since the McMaster MBE system is not currently configured to utilize aluminum based materials, it is impossible to grow AlGaAs/GaAs lasers. However, suitably large bandgaps can be achieved from the InGaAsP material system when it is lattice matched to GaAs. Although this is a relatively unexplored material system for diode laser design, there are several examples where InGaAsP/GaAs lasers have been successfully fabricated. Many of these lasers were designed to operate

at 980 nm to pump Er doped fiber amplifiers [30, 31, 32, 33, 34], although several have been developed that lase in the 800 - 875 nm range [35, 36, 37, 38, 39] with particular interest at 808 nm, the pump wavelength of Nd YAG lasers [40].

There has been a lot of excitement regarding short wavelength aluminum-free lasers. The primary reason cited for growing these lasers is to avoid the reliability problems traditionally associated with aluminum containing lasers. Although catastrophic optical mirror damage resulting from facet oxidation of the aluminum containing materials can be effectively eliminated by surface passivation or AR/HR coatings, formation of dark line defects throughout the device is still a concern [32]. In contrast, InGaAsP based lasers have shown superior reliability regarding the propagation of defects throughout the crystal under extended use [38, 41]. Thus, new short wavelength aluminum free diode laser designs are of significant scientific relevance.

3.1.2 Efficiency and Threshold

There are clearly many benefits to having a laser run with high efficiency and a low threshold. Both properties are a function of the active region design, the ridge width, crystal properties, and cavity length of the laser. Thresholds in the 20 mA to 30 mA range were deemed to be acceptable for this project given that there is a tradeoff between exceptional efficiency and power handling. This tradeoff results from the fact that efficient devices often have narrow active regions. This is done to confine the optical mode such that it strongly overlaps with the quantum wells. However, higher power designs require broader optical modes to avoid localized heating of the active region.

Regardless of the tradeoffs relevant to active region design, poor threshold and efficiency are often caused by poor material quality. If the semiconductor contains impurities or defects, nonradiative recombination centers will deplete the active region of carriers that could be used to pump the lasing transition. Instead, energy resulting from the nonradiative transition is dissipated as heat. This is a serious problem for high power designs since device overheating is usually the dominant power limitation.

3.1.3 Beam Properties

A diode laser's beam properties are entirely determined by the waveguide design. Because the active region is much smaller than the ridges, the emitted beam is elliptical. The divergence in the major axis is determined by the active region thickness and the index of refraction contrast between the core and cladding layers. The waveguiding in the plane parallel to the active region is not nearly as strong and is determined by the ridge width and the lateral effective index contrast. It is necessary to ensure that there is sufficient lateral waveguiding for the laser to be index guided. However, if the index contrast is too strong, and the ridge is too wide, the laser will run on multiple spatial modes. These issues will be discussed in much more detail in section 3.2, as it is critical to use computer models to simplify the waveguide structure specification process.

If a laser is designed such that it has excellent efficiency, but emits a highly divergent elliptical beam that requires additional complex optics to collimate, it is difficult to test and of little use in applications that rely on beam quality. Therefore, good beam properties are particularly important. "Good" in this case is defined to be a single

spatial mode far field pattern with major axis divergence no greater than about 30°. Such a beam represents a good balance between being satisfactorily easy to collimate and being achievable without significantly sacrificing other properties of the laser.

3.1.4 High Power

A number of issues must be considered in order to obtain high power pulses from a laser diode. The saturation energy presents a fundamental limitation to the amount of power produced by a laser. Referring to equation (2.4), the saturation energy of a gain or absorber section is directly proportional to the cross-sectional area of the optical mode. Thus, by increasing the waveguide cross-sectional area, it is possible to increase the saturation energy for the laser. This has the added benefit of reducing the possibility of failure through catastrophic optical damage (COD). By spreading the total beam intensity over a larger cross-sectional area, the intensity at any point can be maintained below the COD threshold intensity for the semiconductor (typically several MW/cm^2).

Obtaining ultimately high powers is not a concern in the first phase of laser development, since much can be learned from studies of mode locking at low powers. Therefore, more sophisticated high power waveguide designs were deemed unnecessary at this stage. However, it was desirable that the devices would be capable of operating over a reasonably large region of pump currents between threshold and thermal rollover. To achieve this, a laser should have low levels of non-radiative recombination centers and deep enough wells that carriers are unable to escape thermally.

3.1.5 Modulation Bandwidth

In order to actively mode lock the diode laser, it must be possible to modulate it at high speeds. For the diode laser in an external cavity, the necessary frequencies will range from hundreds of megahertz to several gigahertz. Typical laser diodes are easily modulated at these frequencies. However, if the laser is to be driven with an ultrashort electrical pulse, the modulation bandwidth must be wide enough that the diode is able to respond to the higher harmonics in the pulse. For actively driven monolithic devices, having a wide modulation bandwidth becomes increasingly important. Although it is possible to couple frequencies higher than the modulation bandwidth (-3dB point) into the laser, doing so requires that more RF power be supplied. Much of the increased RF power ends up contributing to device heating, thereby possibly reducing the device lifetime. Hence a wide modulation bandwidth is important.

The modulation bandwidth is primarily determined by device parasitics which are a function of the contact geometry [42]. Reduced contact areas can significantly reduce the capacitance, thereby increasing the modulation speed. It is easy to reduce the contact regions by simply designing a new mask that only allows the gold contact material to be deposited over the waveguide structure and in a small contact region for bonding. For convenience of testing and fabrication, the initial laser designs have been produced using a standard mask that allows gold coating on most of the top surface of the laser. However, it may be beneficial to incorporate reduced size contacts in later designs.

Intrinsic properties of the laser also impose an upper limit on the modulation bandwidth. Since the resonance frequency is proportional to the square root of the differential gain, lasers with high differential gain should exhibit improved modulation bandwidth [43]. Fortunately, quantum well lasers, and particularly strained quantum well lasers have large differential gains and hence should be well suited to high speed designs. At higher optical powers, increasing gain compression causes the modulation response to become overdamped, which often strongly affects the cutoff frequency. A more detailed analysis shows that carrier transport effects in a separate confinement heterostructure (SCH) play a significant role in the modulation bandwidth of quantum well lasers. The result is that a large undoped SCH waveguide region can significantly reduce the modulation bandwidth [16]. Since a broad waveguide is often desirable in high power designs, this represents a trade off between speed and power.

3.2 Laser Modeling and Design

In order to efficiently design a successful new laser without many costly iterations of fabrication and testing, it is necessary to run computer simulations of possible designs. Assuming the computer model is accurate, running these tests allows one to understand how varying each design parameter affects the properties of the device.

3.2.1 The Model

The computer model used was a modification of a program [44] based on the effective index method as applied to a rectangular dielectric waveguide [45]. Such a model is a good description of several laser waveguide types, including the buried

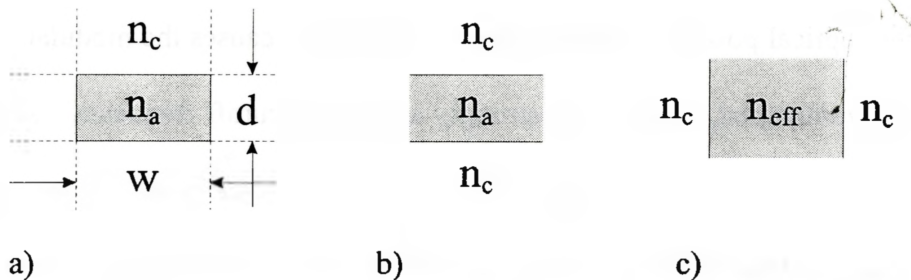

Figure 3.1: Effective index technique for a rectangular dielectric waveguide. The waveguide cross-section (a) is first solved through the epitaxial layers (b) and then (c) laterally using the effective index.

heterostructure. This method works by breaking the rectangular waveguide (as shown in figure 3.1(a) with an active region of index n_a, thickness d, width w, and a cladding index n_c) into two slab waveguide problems that are easier to solve. First, an effective index (n_{eff}) is determined for the active region by solving the slab waveguide through the epitaxial layers as shown in figure 3.1(b). The second slab waveguide problem replaces the active region index with the effective index and solves parallel to the epitaxial layers as depicted in 3.1(c). The far field pattern is then calculated by determining the diffraction of the near field as described by Zeng and Naqwi [46].

Although buried heterostructures are convenient to model, they are not as easy to fabricate due to the requirement of a regrowth after etching. Instead, ridge waveguides were used to provide the lateral optical confinement for all the lasers discussed in this thesis. These structures were chosen because of their good properties and relative ease of manufacture. The cross-sectional profile of such a waveguide structure is shown in figure 3.2. Because a ridge waveguide does not have a defined index step in the plane of the active region (y direction), the simple rectangular waveguide model is inappropriate to use for these lasers. The code was therefore modified to account for this new waveguide structure based on a method described by Kawaguchi [47].

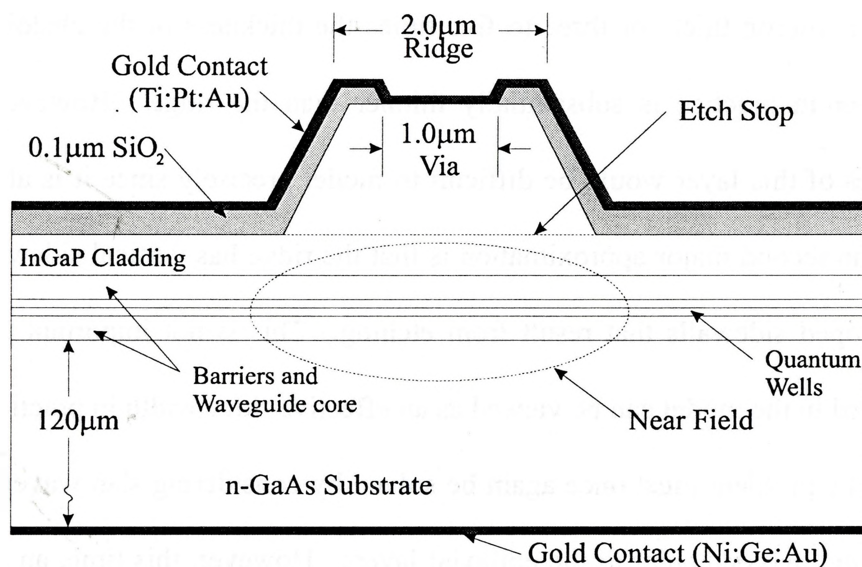

Figure 3.2: Ridge waveguide structure.

The simplified ridge structure used in the model is shown in figure 3.3 (for a ridge of index n_r and width w bounded by two regions of index n_{SiO2} with an upper cladding layer of thickness d_c and index n_c, active region of thickness d and index n_a, and a "substrate" of index n_s). Two major approximations are made, making the problem significantly easier to solve. The first is that the layers above the cladding region all extend to infinity. This is reasonable for the ridge as it is typically about one micron thick, or three to five times the thickness of the cladding layer. The SiO_2 layer in practice is substantially thinner than the ridge. However, the guiding properties of this layer would be difficult to model precisely since it is also coated with gold. The second major approximation is that the ridge has vertical sidewalls in contrast to the sloped sidewalls that result from etching. This is not important since the ridge width used in the model can be viewed as an effective ridge width in practice.

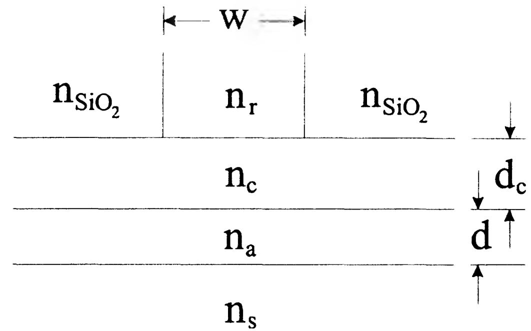

Figure 3.3: Simplified ridge waveguide structure for the model.

The problem must once again be solved by considering slab waveguide solutions parallel and perpendicular to the epitaxial layers. However, this time, an effective index must be found for two regions as depicted in figure 3.4 a): the part under the ridge (I), and the part not under the ridge (II).

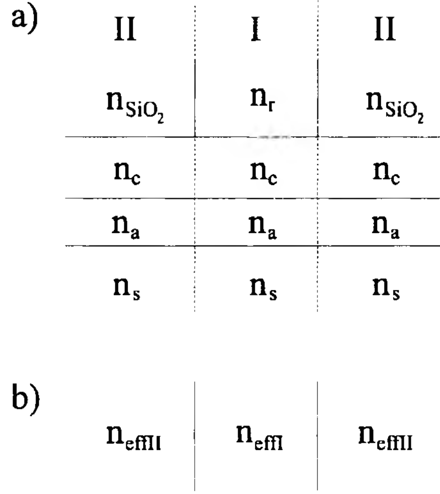

Figure 3.4: The effective index method, applied to a ridge waveguide.

Starting with region II, the first step to determine the effective index n_{effII} is to solve the mode equation for a 4 layer slab waveguide for the wavevector k_x. From Kawaguchi [47]:

$$k_x d = \tan^{-1}\left(\sqrt{\frac{k_0^2\left(n_a^2 - n_s^2\right)}{k_x^2} - 1}\right) + \tan^{-1}\left(\eta\sqrt{\frac{k_0^2\left(n_a^2 - n_{SiO_2}^2\right)}{k_x^2} - 1}\right) + m\pi \tag{3.2}$$

where m={0, 1, 2, ...}, and defined to simplify the expression (3.2),

$$\eta = \frac{\sigma_2}{\sigma_4}\left(\frac{1+T}{1-T}\right) \tag{3.3}$$

$$T = \frac{\sigma_4 - \sigma_2}{\sigma_4 + \sigma_2}\exp\left(-2d_c\sigma_2\right) \tag{3.4}$$

where,

$$\sigma_2 = \sqrt{k_0^2\left(n_a^2 - n_c^2\right) - k_x^2} \tag{3.5}$$

$$\sigma_4 = \sqrt{k_0^2\left(n_a^2 - n_{SiO_2}^2\right) - k_x^2}\ . \tag{3.6}$$

The waveguide propagation constant β_{II} can then be determined,

$$\beta_{II} = \sqrt{k_0^2 n_a^2 - k_x^2} \tag{3.7}$$

and from that, the effective index can be calculated as,

$$n_{effII} = \beta_{II} / k_0\ . \tag{3.8}$$

The approach for region I is identical to that for region II except n_{SiO_2} is replaced by n_r in all the expressions. The regions above and below the etch stop are typically of the same composition with slightly different doping levels. This makes it reasonable to set n_r=n_c in the model. This turns the region under the ridge into a simple slab waveguide problem. However, to maintain generality, the code solves both sections as four layer waveguides and the same numerical value is entered for the variables n_r and n_c.

Once solutions have been obtained perpendicular to the active region, the propagation characteristics for the slab waveguide parallel to the epitaxial layers must be determined using the effective indices of the two regions as shown in figure 3.4 b). First the wavevector k_y must be found:

$$k_0^2\left(n_{effI}^2 - n_{neffII}^2\right) = k_y^2\left[1 + \left(n_{effII}/n_{effI}\right)^4 \tan^2\left(k_y d/2\right)\right] \tag{3.9}$$

The waveguide propagation constant β and cladding decay constant γ can then be determined:

$$\beta = \sqrt{k_0^2 n_{effI}^2 - k_y^2} \tag{3.10}$$

$$\gamma = \sqrt{\beta^2 - k_0^2 n_{effII}^2} \,. \tag{3.11}$$

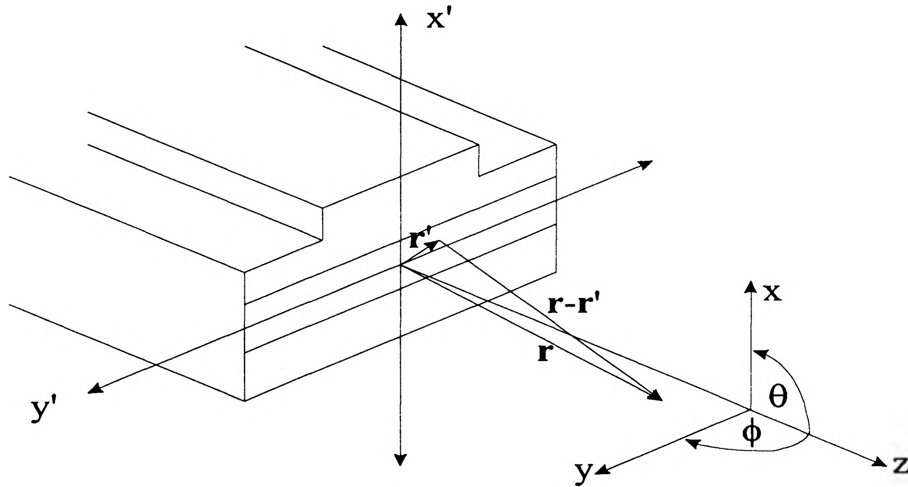

Figure 3.5: Coordinate system used in the far field calculation.

The final step is the calculation of the far field pattern once the near field is determined. This is accomplished by summing the contribution of each near field element $u_n(x',y')$ at a point in the far field of the laser $u_f(x,y,z)$ as shown in figure 3.5. Under the approximations $|\mathbf{r}|\approx|\mathbf{r}-\mathbf{r}'|$ and $|\mathbf{r}-\mathbf{r}'|>>\lambda$, this involves computing the integral (from [46]):

$$u_f(x,y,z) = -\frac{jz}{\lambda r}\frac{\exp(jkr)}{r}\int_{-\infty}^{\infty}\int_{-\infty}^{\infty} u_n(x',y')\exp\left[-\frac{jk}{r}(xx'+yy')\right]dx'dy' \tag{3.12}$$

where $r=|\mathbf{r}|$ and $k=2\pi/\lambda$. Because $u_n(x',y')$ is separable into TE and TM modes, the integral can be broken down into the product of two separate integrals which are much more easily solved. After some mathematical manipulation and transformation into spherical coordinates, the solution for the far field distribution is of the form:

$$u_f(r,\theta,\phi) \propto Au_{fTE}(r,\theta,\phi) \times Bu_{fTM}(r,\theta,\phi), \tag{3.13}$$

where the contribution to the far field from the TE mode is:

$$u_{fTE}(r,\theta,\phi) = 2\cos\left(k_x \frac{d}{2}\right) \frac{\alpha \cos\left(k \frac{d}{2} \sin\theta\right) - k \sin\theta \sin\left(k \frac{d}{2} \sin\theta\right)}{\alpha^2 + k^2 \sin^2\theta} + \frac{\sin\left(\left(k_x - k\sin\theta\right)\frac{d}{2}\right)}{k_x - k\sin\theta} + \frac{\sin\left(\left(k_x + k\sin\theta\right)\frac{d}{2}\right)}{k_x + k\sin\theta} \tag{3.14}$$

with α as the cladding decay constant perpendicular to the active region:

$$\alpha = \sqrt{\left(\sigma_2^2 + \sigma_4^2\right)/2}\,. \tag{3.15}$$

The TM component of the far field is similar except that each occurrence of k_x is replaced by k_y, α with γ, and θ with ϕ.

The intensity at a point is simply the square of the far field amplitude, so the intensity profile of the beam can be determined by sweeping θ or ϕ. The code then finds the angle corresponding to the full width at half maximum of the intensity profile.

To optimize the waveguide to meet the design criteria, the index of the active region and cladding along with their dimensions are adjusted. The amount of guiding can be reduced by using a low index contrast waveguide with a large core. However, if the guiding is too weak, the laser will behave more like a gain guided broad area device. Additional constraints are put on the dimensions of the cladding thickness between the etch stop and the active region. As the thickness of this region is reduced, the ridge plays a stronger role in the lateral confinement of the guided mode by introducing a stronger effective index contrast. Thus, by suitably adjusting the various parameters, an optimal solution can be obtained.

3.2.2 Active Region Design

The computer model discussed above is used to optimize the waveguide to work with a given active region design. Although the quantum wells are not directly considered in the waveguide calculations, they provide constraints for the band gap range of the barriers in the active region, and this material forms the core of the waveguide. So, the first step in the laser design process is to choose the number of quantum wells and the material out of which they are to be made.

As mentioned in subsection 3.1.1, the material used for the quantum wells is dictated by the wavelength choice for the laser since the transition energy corresponds to the photon energy. A more detailed analysis of the quantum well transition energies is necessary to assist in the choice of the quantum well thickness and composition. In general, quantum wells can support many energy levels. However, it is beneficial to design the well's depth such that only one transition is allowed to ensure that there will not be competing transitions. Additionally, it is important to ensure that the well is deep enough that carriers are not able to easily escape thermally.

The energy levels in a finite square well with a barrier height V_0 and width L can be found by solving [45]:

$$\frac{\sqrt{2m_b(V_0-E)}}{\hbar}=\frac{m_b k}{m_w}\tan\left(k\frac{L}{2}\right) \tag{3.16}$$

for even wavefunctions and

$$\frac{\sqrt{2m_b(V_0-E)}}{\hbar}=\frac{m_b k}{m_w}\cot\left(k\frac{L}{2}\right) \tag{3.17}$$

for odd wavefunctions, where

$$k = \frac{\sqrt{2m_w E}}{\hbar} \tag{3.18}$$

and m_b and m_w are the effective masses in the barriers and wells respectively. The number of bound states (N) in the well can be found using:

$$(N-1)\pi/2 \leq \sqrt{2m_w V_0}\left(L/2\hbar\right) \leq N\pi/2\,. \tag{3.19}$$

Since the effective masses of the electrons, heavy holes, and light holes are different, the energy levels for each must be calculated separately.

These energies represent the energies from the bottom of the well. Thus, the transition energy can be calculated for each transition by adding the band gap energy (E_{gw}) to the sum, as is evident in figure 3.6. It is important to note that the depth of the valence and conduction band wells are not equal ($\Delta E_c \neq \Delta E_v$) and so the number of levels supported by each is not necessarily the same. Typically the difference in the well and barrier band gaps is split roughly 40%/60% between the conduction and valence bands respectively.

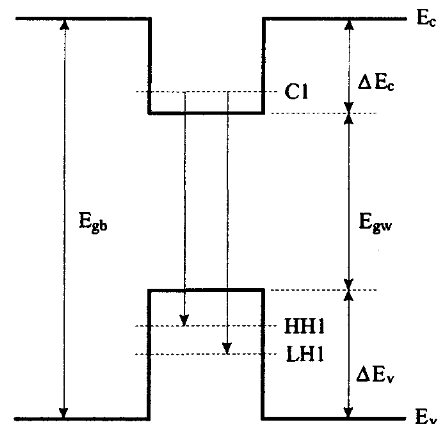

Figure 3.6: Quantum well energy levels.

In general, it is beneficial to introduce a small amount of strain into the quantum wells, since strained wells typically have lower carrier densities at transparency and higher differential gains [43]. When a thin layer of semiconductor is grown on bulk material of a slightly different lattice constant, the crystal lattice of the thin layer will

deform to try to match the lattice constant of the bulk material along the interface. The two components of the resulting strain in the thin layer alters the band gap energy for the quantum well. This is given by [48]:

$$\Delta E_{hh} = -2a\varepsilon\left(\frac{C_{11} - C_{12}}{C_{11}}\right) + b\varepsilon\left(\frac{C_{11}+2C_{12}}{C_{11}}\right) \tag{3.20}$$

$$\Delta E_{lh} = -2a\varepsilon\left(\frac{C_{11} - C_{12}}{C_{11}}\right) - b\varepsilon\left(\frac{C_{11}+2C_{12}}{C_{11}}\right) \tag{3.21}$$

where the C_{ij}'s are the elastic stiffness coefficients, a and b are the hydrostatic and shear deformation potentials respectively, and the lattice mismatch is defined as:

$$\varepsilon = \frac{a_w - a_b}{a_w} \tag{3.22}$$

where a_w and a_b are the lattice constants of the wells and barriers respectively. These energy shifts are added to the band gap energies prior to calculating the transition energies.

3.2.3 Quaternary Interpolations

This methodology of laser modeling relies heavily on accurately knowing the index of refraction for each region of the laser in order to specify the waveguide. Therefore, it was necessary to go to some lengths to obtain accurate estimations of the index of refraction for each material as a function of bandgap or composition. Due to the great deal of research that has been done in developing lasers for telecommunications applications, there exists an abundant data base for InGaAsP quaternaries as deposited lattice matched to InP substrates [49, 50, 51]. Unfortunately, such a data base for the

index of refraction quaternaries lattice matched to GaAs is almost non-existent. Thus, a thorough study of the index of refraction of quaternaries deposited on GaAs would be of great benefit to designers of short wavelength InGaAsP/GaAs lasers.

Because of the inadequate data available in the literature, it was necessary to use an interpolation scheme to make use of the more accurately measured binary data. The simplistic approach would be to directly linearly interpolate the index of refraction by composition of $In_{(1-x)}Ga_xAs_yP_{(1-y)}$ (Vegard's rule):

$$n = n_{InP}(1-x)(1-y) + n_{InAs}(1-x)y + n_{GaP}x(1-y) + n_{GaAs}xy \tag{3.23}$$

This does not work very well, however, since the index and band gap vary in a somewhat nonlinear fashion. This deviation from linearity is referred to as bowing [52, 53]. Instead it is preferable to use Vegard's rule to interpolate the following expression as discussed by Burkhard et al. [49]:

$$\gamma = \frac{\varepsilon - 1}{\varepsilon + 2} \tag{3.24}$$

where the ε's are the dielectric constants of the binary components. These have been accurately measured using spectroscopic ellipsometry for the range of 1.5 eV to 6.0 eV in steps of 0.1 eV by Aspnes and Studna [54]. The index of refraction is then calculated using $n^2 \approx \varepsilon$, or:

$$n = \sqrt{\frac{2\gamma + 1}{1 - \gamma}}. \tag{3.25}$$

When depositing the epitaxial layers by MBE, the compositions are specified by the effective bandgap (E_{PL}) of the material deposited. So, in order to specify a laser

design when submitting a growth request, it is necessary to convert the desired composition to a band gap in electron volts. A curve fit for Pessa's lattice match data [55] was used in order to achieve this:

$$E_{PL} = 1.995 - \sqrt{0.3129y + 9.724 \times 10^{-3}}\,. \tag{3.26}$$

The wavelength corresponding to a given bandgap is then $\lambda = hc/E_{PL}$. Once a material is grown, its photoluminescence (PL) spectrum is measured to determine if the material was grown with the correct bandgap. This makes it possible to ensure that the properties of the waveguide designed on the computer correlate well with the properties of the fabricated lasers within the uncertainties of the quaternary physical data.

3.3 Measurement Apparatus

All of the quarter wafer blocks of processed lasers were cleaved into laser bars for testing. This is the most convenient form for facet coating using the ECR-CVD system. In order to facilitate testing before and after coating, a test configuration was designed to study laser bars. This consisted of a copper block cooled by a thermoelectric cooler on a large aluminum heatsink. The copper blocks and heatsink were designed such that lenses could be easily positioned very close to either facet of the laser, as is shown in figure 3.7. This makes it possible to optimally couple light from the back facet into an external cavity while obtaining a nicely collimated beam from the front facet. The copper block's temperature was controlled to a high degree of stability with the thermoelectric cooler section of an ILX LDC-3732 laser diode controller.

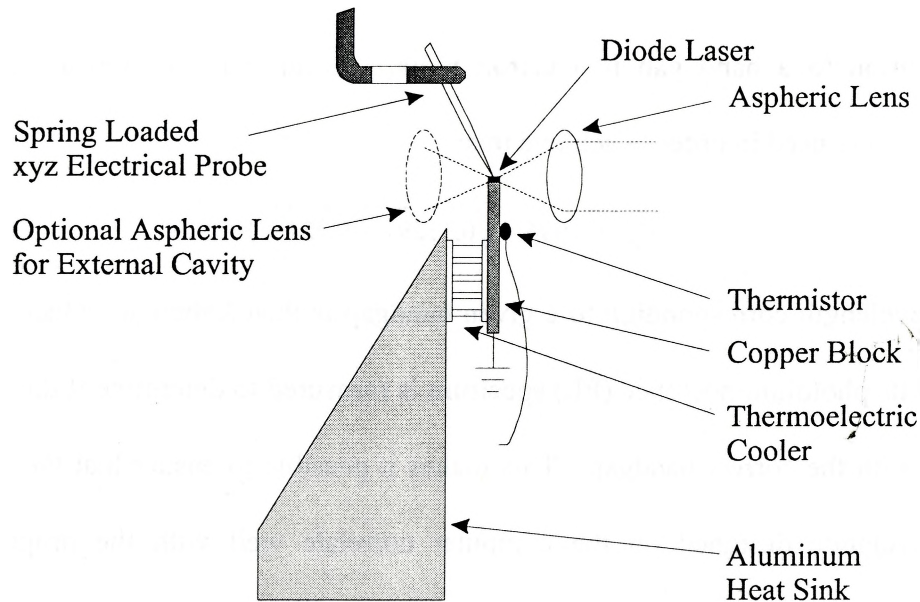

Figure 3.7: Diode laser test configuration.

One of the most basic measurements used to characterize diode laser performance is the light vs. current (LI) characteristic. For this measurement, a large area silicon photodiode detector was positioned within 2 mm of the unfocussed output of the laser facet. This gave more repeatable results than measuring the focused beam directly while simultaneously allowing more rapid measurement of multiple lasers, by avoiding the need to realign a lens. Software was created to automate the measurement of LI curves on the computer by controlling the ILX current controller via a GPIB interface and measuring the photodiode signal with a 12 bit AD converter board in the computer.

3.4 980 nm Lasers

Single Quantum Well (SQW) InGaAsP/GaAs lasers emitting at 980 nm have previously been designed, grown, and processed at McMaster [34]. The knowledge

developed from this work could therefore be used as a starting point for our own research. Our group had obtained some of these lasers for initial studies, so we had a good understanding of their strengths and weaknesses. The laser design found to be most successful by these researchers is shown in figure 3.8.

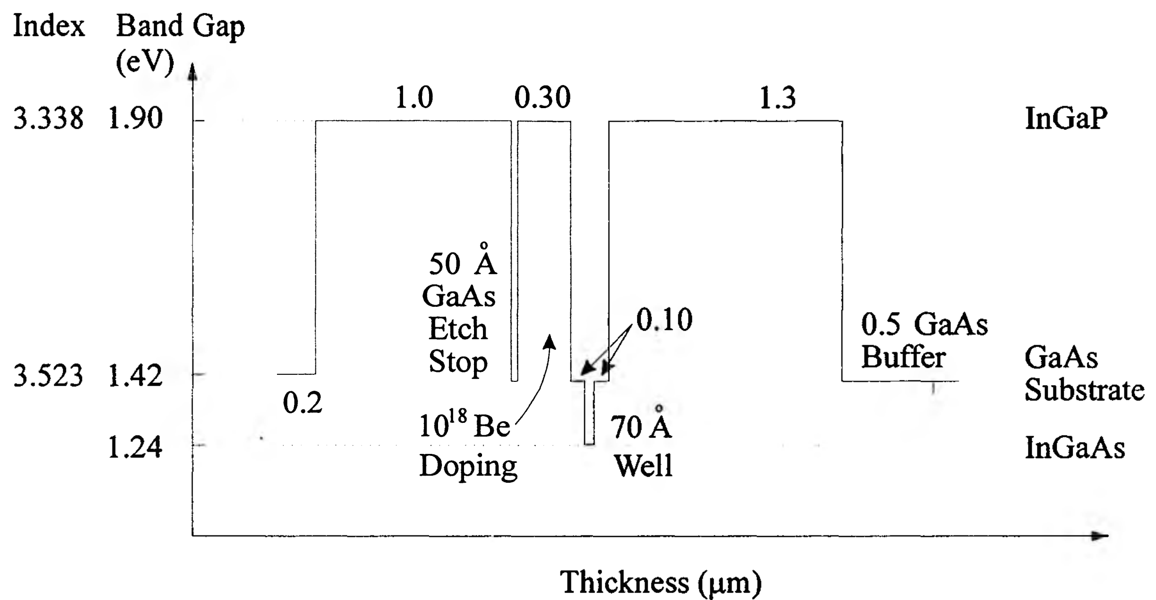

Figure 3.8: The band structure of the existing SQW 980 nm laser design.

The primary weakness of these lasers from our perspective was that their beam was highly divergent along the vertical axis. This highly elliptical beam was difficult to focus and therefore was not ideal for use in an external cavity. The reason for this divergence was that the index contrast between the core and cladding of the waveguide was very high, so the light was too heavily guided. This may have helped to improve the threshold and efficiency of the devices, but at the expense of having a good far field pattern. Therefore, the index of refraction and thickness of the active region were modified in order to improve on this aspect of the laser's performance.

The other characteristic of the existing 980 nm design that needed to be modified was the resistance between contacts. In order to have multiple contact lasers that have well isolated sections, there must be a high resistance between the contacts of the laser. The actual current flow in a multiple contact laser is complicated to model. However, from basic electronics, the resistance of a conductor can be increased by increasing the resistivity of the material and decreasing its cross-sectional area. In this case, the resistivity was increased by decreasing the level of doping of the cladding layer below the etch stop while simultaneously reducing the layer's thickness. There are several tradeoffs involved in modifying this layer. The layer should be highly doped to ensure low resistance between the contacts and the active region. Reducing the thickness of this layer can compensate for that. However, if the cladding layer is too thin, the ridge provides too much guiding for the light in the active region of the laser. Thus, a suitable combination of the two approaches is necessary to find an optimal combination of contact isolation, waveguiding, and electrical conductivity into the active region.

The final design of the 980 nm lasers is shown in figure 3.9. There are several important differences between this design and the existing 980 nm lasers. The most significant change was the modification of the waveguide core. The existing 980 nm lasers used GaAs for the waveguide for simplicity of growth. A quaternary with a peak PL signal at 783 nm was developed for the new 980 nm lasers in order to reduce the index contrast of the core of the waveguide. The index of refraction of this material was calculated to be approximately 3.44 as compared to 3.52 for the GaAs used for the core of

the old SQW design. Both designs use InGaP for the cladding, with an index of refraction of 3.34. The core of the waveguide is also wider than the old design as it contains two quantum wells and a slightly wider waveguide region on either side of the wells. The combination of the higher index active region and wider waveguide produced an improved far field pattern both in theory and practice. The theoretical divergence along the major axis of the beam for the new laser design was 30.6° as compared to 44.5° for the existing lasers.

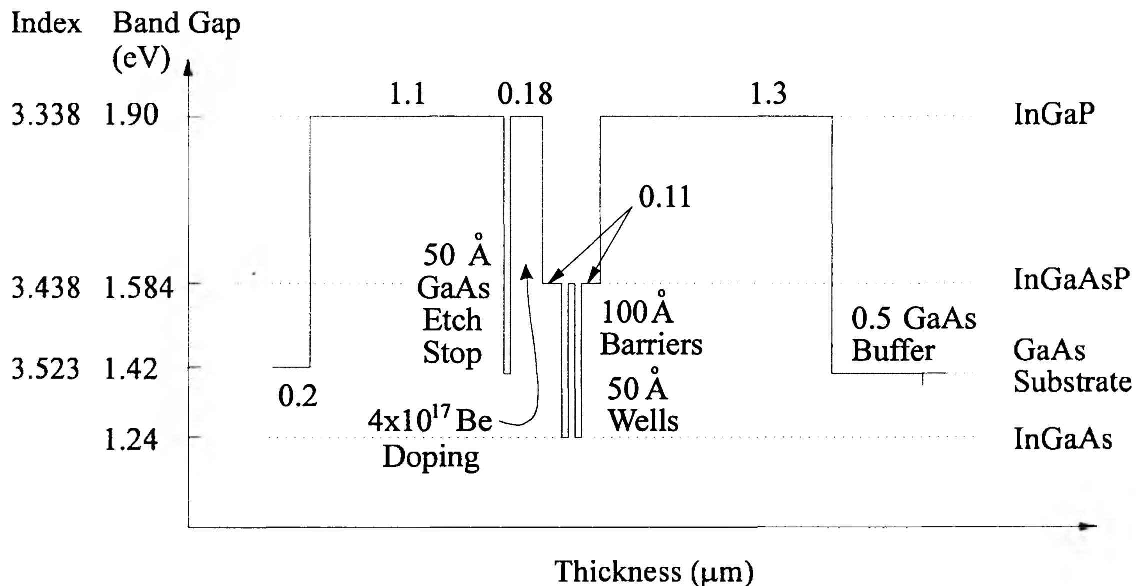

Figure 3.9: The band structure for 980 nm lasers from growth #2391. The quaternary had an approximate composition of x=0.585 and y=0.140 ($In_{1-x}Ga_xAs_yP_{1-y}$).

The other major modification was the adjustment of the cladding layer below the etch stop. The resistance of this layer was significantly increased by decreasing the resistivity by a factor of two and the thickness by almost the same amount. Typical resistances between contacts of split contact lasers processed from this growth were on

the order of 1 kΩ. Split contact lasers of the old design had resistances of approximately 500 Ω.

In spite of these differences between the designs, the layers above the etch stop were essentially unchanged. This allowed the lasers to be processed according to the procedure developed for the existing design [56]. It is important to note, however, that an unforeseeable problem occurred during processing which resulted in lasers with the deformed ridge structure as shown in the SEM image of figure 3.10. This is a result of the waveguide structures being aligned along the [011] crystal axis instead of the [01$\bar{1}$] axis. This was because the GaAs wafers used had reversed major and minor flats (European/Japanese instead of American). Since the etch rates for the two crystal directions are different, the processing recipe, designed to produce optimally etched sloped sidewalls for the ridges, instead did so for the features perpendicular to the ridges while undercutting the sidewalls. This was confirmed by an SEM image of a feature perpendicular to the ridge (figure 3.11).

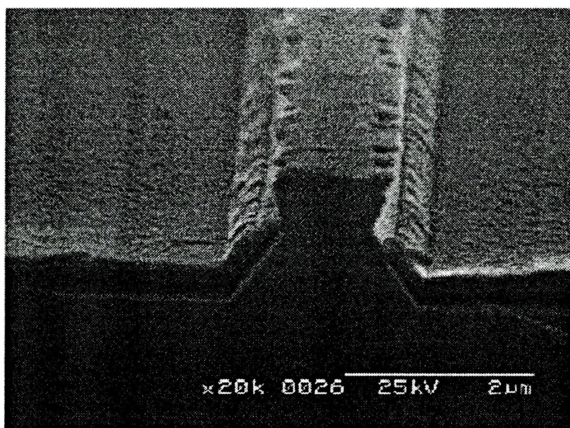

Figure 3.10: Ridge of a 980 nm laser.

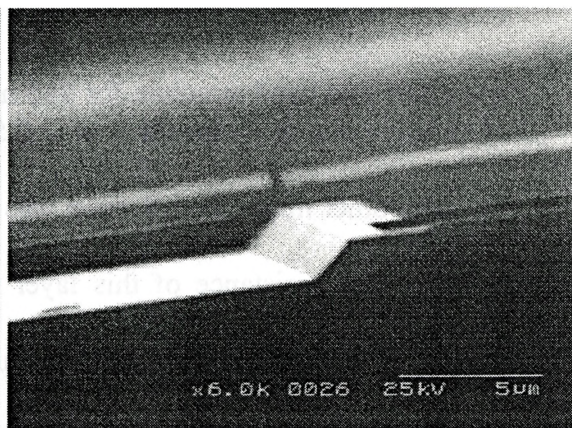

Figure 3.11: Feature perpendicular to ridge.

In spite of the oddly shaped ridge, the lasers lased with low thresholds and quite good efficiencies. A plot of LI curves for lasers with several ridge widths is shown in

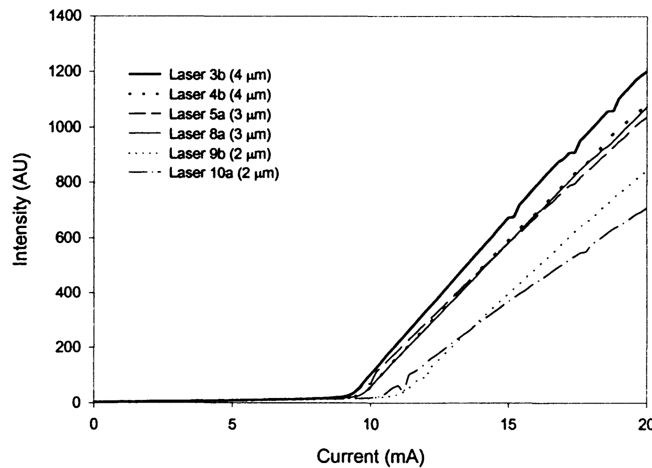

Figure 3.12: Typical LI curves for several ridge widths of lasers from growth 2391.

figure 3.12. The thresholds for these lasers are comparable to those of the SQW design, although the efficiency is somewhat lower. This was expected since the optical mode is less confined in the new design, thereby interacting less with the wells. However, the lasers were expected to exhibit less rollover at high powers since the deeper quantum wells should reduce the thermal loss of carriers. As is shown in figure 3.12, the lasers did not exhibit thermal rollover for the limited range of currents over which they were tested without failure.

It was evident fairly early on that these lasers were not quite as reliable as desired. It was observed that as the current was increased, the LI curves did not roll off like the existing SQW lasers, but rather, continued linearly upwards until the lasers failed

completely. Examination of the lasers after such a test clearly showed that parts of the ridge had melted. An SEM image of the ridge of one of these lasers is shown in figure 3.13. A closer look at a laser that failed near the facet clearly shows that the ridge is removed below the etch stop through to the active region (figure 3.14).

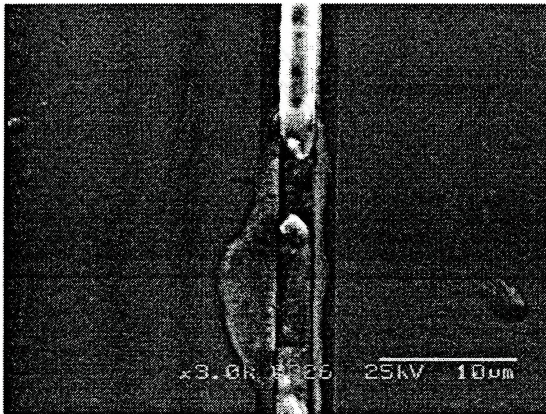

Figure 3.13: A damaged ridge.

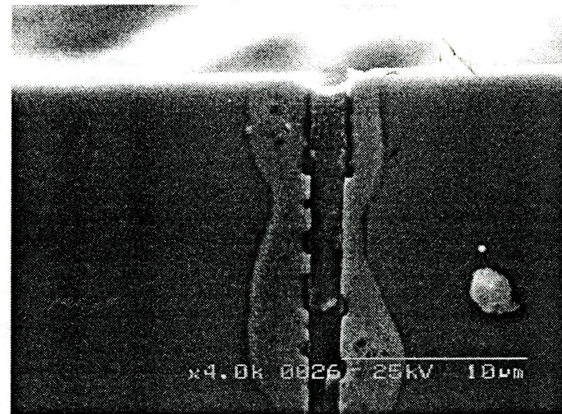

Figure 3.14: Ridge damage near facet.

The expected cause of the melting of the ridges is related to the line of sight deposition of other materials on top of the hourglass shape. Shadowing of some of these layers by the underside of the hourglass can be clearly seen in figure 3.10. The first of these is an insulating layer of SiO_2. This should have been deposited everywhere and then later etched through along the ridge to provide an electrical contact. Instead, the underside of the undercut was not coated, allowing current to flow into the ridge from the sides. After the vias were etched, titanium and platinum layers were deposited to provide a diffusion barrier for the gold contact layer. Again, the titanium and platinum layers likely did not deposit on the underside of the ridge. However, because the gold layer was deposited with the sample stage tilted at a 50° angle, the undercut region was gold coated. Because of the lack of titanium and platinum layers, the gold was able to

diffuse freely into the ridge. This would cause a viscious cycle of localized heating leading to an increased diffusion rate, continuing until the ridge became sufficiently hot to melt.

The optical spectra of these lasers were measured above and below threshold using an optical spectrum analyzer. The results are shown in figure 3.15. The lasing wavelength for these devices was close to 995 nm.

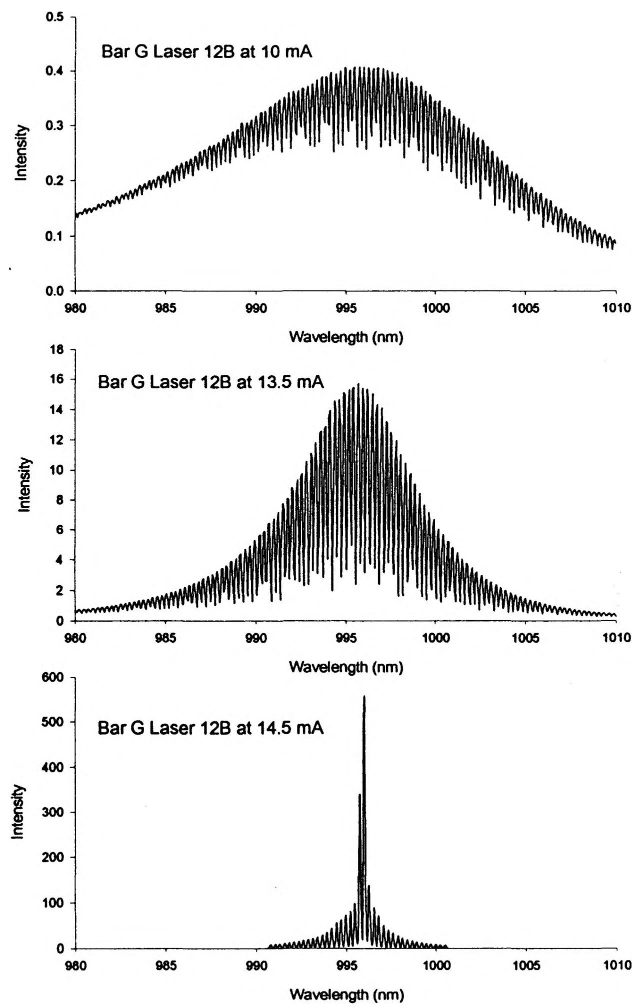

Figure 3.15: Optical spectra of a 980 nm laser.

3.5 850 nm Lasers

As discussed in section 3.1.1, moderately short wavelength ultrafast lasers are particularly important because they are necessary for many two photon applications. Hence, development of an 850 nm InGaAsP/GaAs laser is the next step in that direction. Conveniently, the band gap of GaAs is approximately 850 nm, so one would expect that a design using GaAs quantum wells would be an effective way to produce such a laser. Additionally, the InGaP cladding used for the 980 nm lasers would still be suitable to use since its bandgap of 1.9 eV is much larger than that of GaAs (1.42 eV).

The only other material to be chosen was the barrier region. Since the index contrast from the 980 nm laser was still fairly high, a larger band gap quaternary was needed. Concurrent with the development of the 980 nm lasers, several other quaternaries were grown with strong PL peaks at 705 nm and 795 nm. The composition with PL at 705 nm provided a suitable index of refraction for implementation as the waveguide and barrier region.

Further computer simulations were performed to find the optimal dimensions for a laser grown with these materials. A wider waveguide region was used (0.19 μm as compared to 0.11 μm for the 980 nm lasers) to also reduce the divergence of the beam. The computer model predicted far field divergence for these lasers of 16.0°. The experimentally observed divergence, estimated to be about 30°, was also less than that of the 980 nm lasers. The final design is shown in figure 3.16.

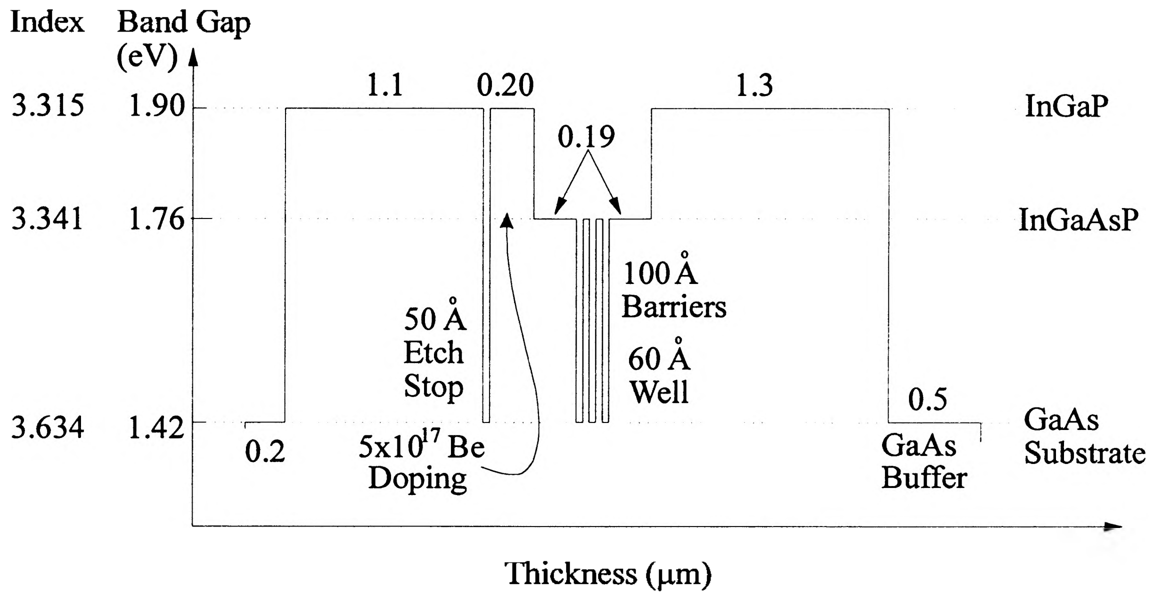

Figure 3.16: The band structure for 850 nm lasers from growth 2486. The quaternary had an approximate composition of x=0.766 and y=0.510 ($In_{1-x}Ga_xAs_yP_{1-y}$).

These lasers were processed using the same methodology as was used for the 980 nm lasers. This was possible because the epitaxial layers from the etch stop up were identical for the two designs. An SEM image of a ridge of one of these lasers is shown in figure 3.17. The cleanly sloped sidewalls confirm that the ridges were processed correctly.

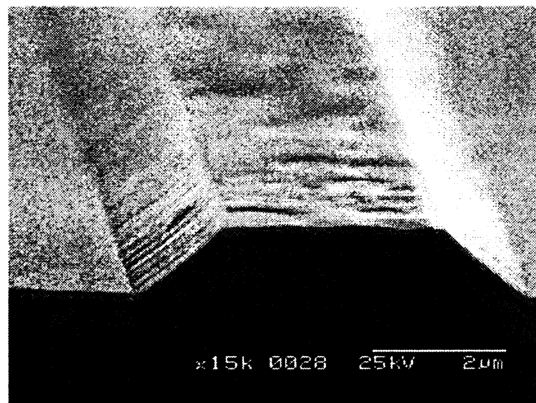

Figure 3.17: The ridge of an 850 nm laser diode.

The lasers lased with typical thresholds of 50 mA, and reasonably good efficiencies. Although this threshold is quite high, there are many commercial lasers that have similar thresholds, so this is not a serious problem. A typical LI curve is shown in figure 3.18 for a 4 μm ridge, 850 nm laser. Approximately 5 mA above threshold, the laser stopped lasing, but continued to emit light. Upon repetition of this experiment, the laser would not lase at all, instead producing spontaneous emission above and below the original threshold current. Similar results were obtained for numerous lasers of the same growth.

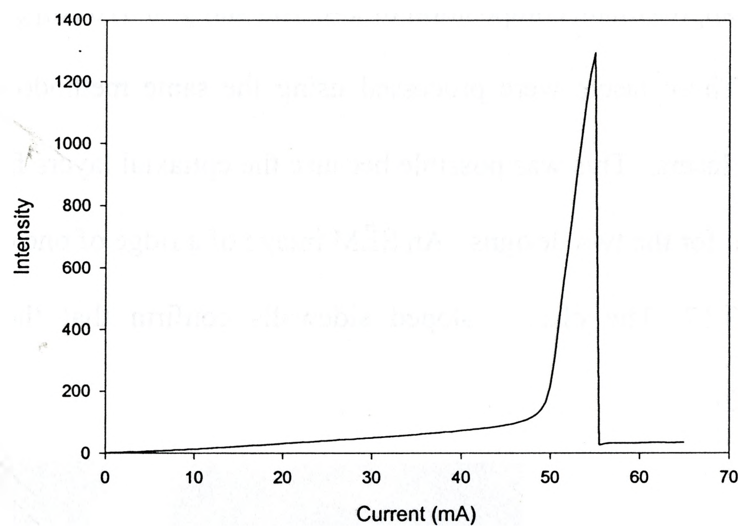

Figure 3.18: A typical LI curve for lasers from growth 2486.

Optical spectra were measured for currents above and below threshold (figure 3.19). These show a significant red shift in the center wavelength for increasing carrier

density. This is to be expected given that a large carrier density was needed to reach threshold. A closer look at the laser above threshold is shown in figure 3.20.

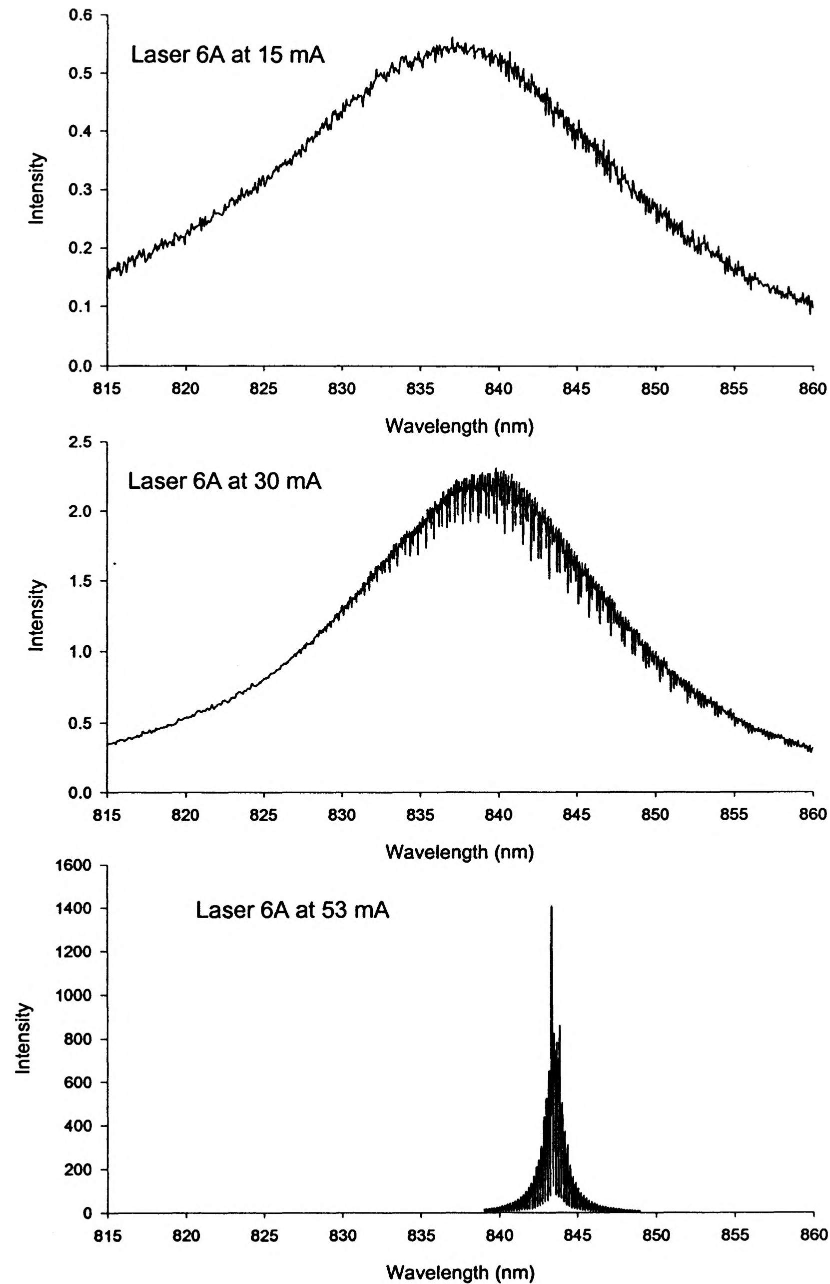

Figure 3.19: Optical spectra of an 850 nm laser.

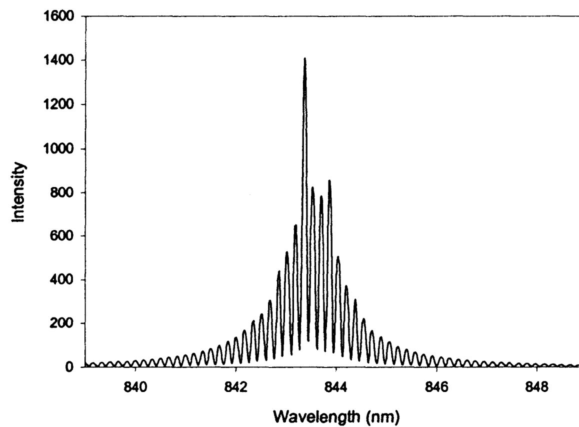

Figure 3.20: An 850 nm laser above threshold (53 mA).

The LI measurements suggest that there is clearly a difference in the failure mechanism for these lasers as compared to the 980 nm lasers. Lasers that had been tested in this way were observed under an optical microscope and by SEM. There was no clearly visible damage on any of the laser facets or ridges after such a failure. Thus one might expect that the undesirable properties of these lasers could be related to the material properties or the design of the epitaxial layers.

The other unexpected characteristic of these lasers was that they emitted red light when injected with current. This occurred above and below threshold and also before and after failure. Careful observation with a microscope revealed that the light was emanating from the laser facets, rather than uniformly along the ridge. Since they were

designed to lase at 850 nm, and the eye is not sensitive to light of wavelengths larger than about 750 nm, it appeared that an unwanted transition was taking place in the device.

The first possible source of a short wavelength transition in the lasers would be the presence of multiple levels in the quantum wells. Hence it was necessary to calculate the transitions available, as discussed in subsection 3.2.2, to ensure that this was not the case. The result was that the wells could only support one heavy hole and one light hole transition. The transition energies were found to be at 1.469 eV (844 nm) for the conduction band to HH transition and 1.490 eV (832 nm) for the conduction band to LH transition. Since the matrix element for the TE polarization for the HH transition (1/2) is larger than for the LH transition (1/6), the laser will almost certainly only lase on the HH transition [16]. Thus one can conclude with reasonable certainty that the quantum wells are not the source of the visible transition.

The materials in the laser having large enough bandgaps to support visible transitions include the InGaP cladding region and the InGaAsP barrier region. Recombination in the cladding is highly unlikely because that region is highly p-doped. Under forward bias, holes are injected through this region. Thus electrons, being minority carriers, are so few that recombination there is negligible. Once carriers reach the InGaAsP barriers, they should immediately be attracted to the quantum wells. Therefore, if the materials properties of the InGaAsP are good, recombination in the barriers should be negligible.

In a certain region of the MBE growth parameter space, the quaternary is unstable energetically due to the difference in bond lengths for the different binary constituents. As a result, localized regions of binary-rich material (InAs and GaP) can form within a layer that has an overall nominal quaternary composition. This is referred to as spinodal-like decomposition [57].

Materials exhibiting spinodal decomposition can behave similarly to reduced dimensional structures. Thus, it is possible for transitions to occur between energy levels in the effective potential wells formed by the localized regions of binary materials. Additionally, one would expect scattering of light in such a material due to the high density of compositional changes. To confirm that spinodal decomposition was the problem, several samples were studied using TEM. Significant amounts of compositional fluctuations were observed, strongly suggesting that this was the source of the red light and poor LI characteristics.

3.6 Future Laser Designs

Clearly, the first area that must be studied in order to produce reliable 850 nm lasers in the future is the MBE growth of quaternaries lattice matched to GaAs over the entire compositional range. Several approaches will be considered to solve the problem of spinodal-like decomposition in these materials. One possible solution is to force a different growth mechanism. It is believed that the growth mechanism on a flat surface is of the island type, possibly leading to preferential islands of InAs and GaP. It would be

desirable to force stepwise growth by using a so-called off-cut wafer, where the top surface is sloped at an angle of 2 or 3 degrees, resulting in a sort of atomic staircase.

Spinodal decomposition of InGaAsP has been characterized for quaternaries lattice matched to InP [57]. A similar study should also be performed to determine the parameter space appropriate for growth of quaternaries lattice matched to GaAs. Conclusions derived from the InP study should be relevant to the GaAs system as well, so in the short term, optimization of growth parameters should be possible. It has been experimentally observed [57] that increased growth temperature increases the level of decomposition, as does a reduced group V flux. This is because the spinodal isotherm, defined as the boundary of the region where the Gibbs free energy surface becomes negative, expands in area under these conditions. Thus, it should be possible to grow the quaternary at somewhat reduced temperatures and increased group V fluxes such that it falls outside the region defined by the smaller spinodal isotherm.

As more quaternaries are grown with improved material properties, lasers may be designed based on a much wider selection of wavelengths using highly optimized waveguiding. The original 980 nm lasers were restricted in their waveguiding properties because of the simplicity of their design using a GaAs SCH region. The development of the 783 nm quaternary made it possible to greatly improve the waveguiding properties of a 980 nm laser. By developing a shorter wavelength quaternary and using GaAs quantum wells, it was possible to realize a functioning 850 nm laser. The next logical step would be to use a quaternary with a somewhat larger bandgap than 1.42 eV (GaAs) for quantum

wells of an even shorter wavelength laser. This would likely require an additional larger bandgap quaternary for the waveguide core.

Eventually, speveral applications will require new laser structures capable of higher powers and wider gain bandwidths. A wider gain bandwidth may be obtained by using multiple quantum wells, with staggered thicknesses combined with interference filters designed to flatten out the gain profile [58]. A wide gain bandwidth is important to permit more modes to be coupled together in order to obtain shorter pulses. Staggered thickness multiple quantum wells can also be used to optimize the overlap of the carrier concentration with the active region [59].

Higher power epitaxial designs will eventually be necessary for laser amplifiers as well as for more powerful lasers. This will be necessary to obtain the high peak power pulses desirable for many applications. There are various active region waveguide modifications that have been found to be successful in producing higher power lasers. Most of these concentrate on reducing the optical power density in the active region in order to prevent catastrophic optical damage. One approach that has been successful in producing high power devices (up to 8 W) is to increase the thickness of the barrier/waveguide region between the quantum wells and the cladding [33]. While this has some drawbacks (reduced modulation response in particular), a somewhat broader waveguide may be advantageous in the future.

In addition to optimizing the active region for higher powers, the waveguiding resulting from the ridge should be optimized as well. Again, it is desirable to increase the

cross-sectional area of the mode to avoid overly high optical power densities in the device. One approach to this that has been successful in high power semiconductor optical amplifier designs is the use of tapered or flared waveguides [60, 61]. In a multisection device, it is possible to use a narrow absorber section with optimally low saturation energy while having a tapered gain section that can handle high powers [62]. Such a laser could be produced in essentially the same way as the ridge waveguide lasers developed so far. The primary change that would be required is that a new mask would need to be made to define ridges with a tapered shape.

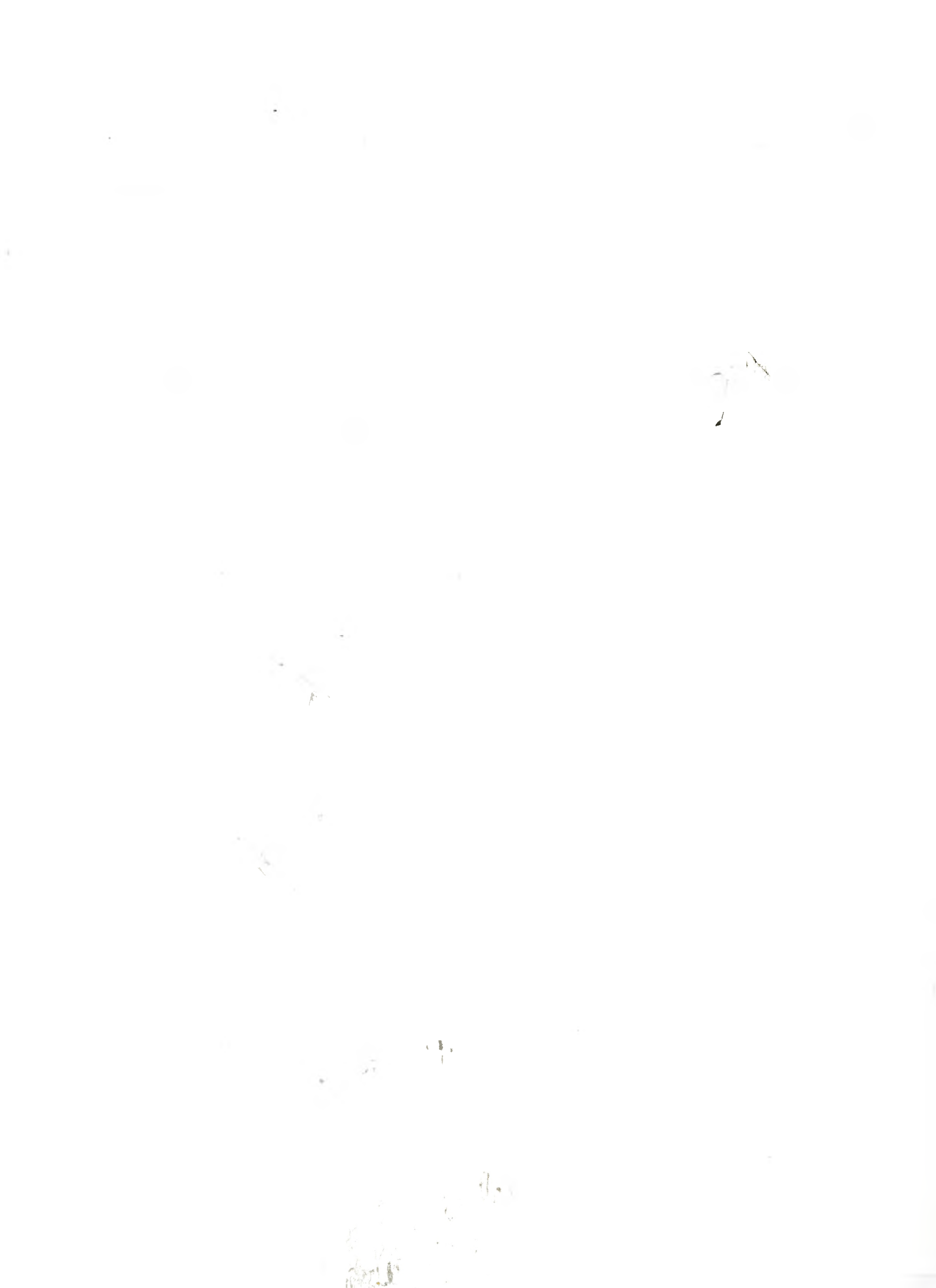

Chapter 4: Split Contact Theory and Characterization

The performance of a passively mode locked semiconductor laser is heavily dependent on the design of the saturable absorber used. For a split contact diode laser, this means that it is critical to optimize the performance of the saturable absorber section. Aside from the material issues that arise when the epitaxial layers are designed, one must optimize the dimensional properties and biasing conditions for the absorbing section. Hence an understanding of split contact theory and device characterization is essential.

4.1 Split Contact Biasing Theory

The extra biasing freedom introduced by a second electrode on the laser significantly complicates the analysis of the laser's performance. It has been observed both experimentally and in theory that biasing these lasers in various regimes can produce effects ranging from normal CW lasing with varying degrees of loss, to self-pulsations in the optical power and hysteresis loops in the LI curve [63, 64, 65]. All of this behaviour can be understood in a qualitative way by considering the electrical biasing of the laser based on the negative differential resistance exhibited by the IV curve of the absorbing section under varying gain section currents.

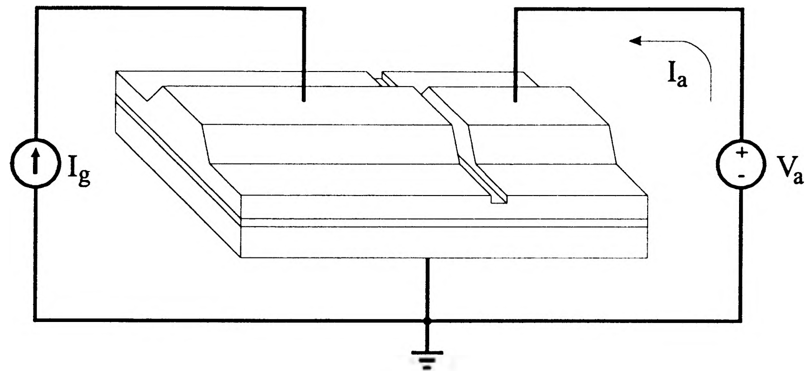

Figure 4.1: Electrical connection to a split contact laser.

Consider a split contact laser composed of two sections as shown in figure 4.1. There is a gain section which is pumped with a current I_g and there is an absorbing section which is biased with a voltage V_a resulting in a current of I_a. When an IV curve is measured for the absorbing section, the total current detected is primarily composed of the sum of two parts: the exponential bias current, as defined by the diode equation, and the photocurrent generated by the absorption of photons created in the gain section [64]. This photocurrent is a function of the current in the gain section as well as the absorber bias voltage, since both parameters determine the net gain or loss for the laser. In addition, a fraction of I_g leaks between the contacts, directly contributing to I_a.

Depending on the device parameters, different combinations of these currents will dominate for different regions of the absorber IV curve. When V_a is negative, the absorption is very strong, resulting in a high cavity loss and limited stimulated emission. Therefore, the photocurrent contribution to I_a is small, resulting only from absorption of gain section spontaneous emission. As V_a is increased, the cavity loss drops and the laser eventually reaches threshold. At this point, the negative photocurrent dominates the

contributions to I_a, producing a "dip" in the IV curve. At larger absorber section voltages, the positive exponential current becomes dominant and the IV curve turns upwards once again. The dip becomes more pronounced as the gain section current is increased, as more photons are generated to be absorbed in the absorber section.

If numerous absorber section IV curves are measured at different gain currents, it is possible to plot a graph not unlike the characteristic curves for a transistor. An example of a set of theoretical IV curves is shown in figure 4.2. One can draw a load line on this graph corresponding to the path taken through the absorber IV space as the gain section current is changed, assuming the absorber bias is set with a defined impedance. The load line's slope is determined by the impedance in series with the absorber section.

Thus, it is possible to select a series resistance for the absorber section such that the load line crosses several constant I_g absorber IV curves twice. An example of such a load line is shown in figure 4.2. When the laser is biased in this way, increasing I_g causes the absorber bias to shift along the load line across the contours. Eventually, there will be a point (A) where the next higher I_g contour will only intersect the load line on the other side of the dip. The IV biasing then jumps over to that part of the curve (B) to satisfy the electrical circuit requirements. However, at this

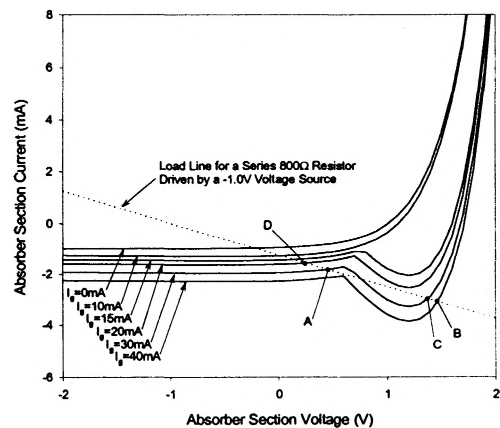

Figure 4.2: Simulated split contact IV curves for different gain section currents.

increased absorber voltage, the absorbing section becomes more transparent, so more photons are generated and a discontinuity appears in the LI curve. When the current in the gain section is then reduced, the light emitted drops smoothly as the absorber bias follows the load line. This continues until it once again has to cross the dip (point C). In general, the return crossing of the dip occurs at a different gain section current. This results in hysteresis of the discontinuity in the LI curve.

The size of the discontinuity and amount of hysteresis are determined by the shape of the dips in the IV contours of the absorber section and the circuit parameters that define the load line. Clearly, if the dips are weak, there will only be a small region of negative impedance, so it would be difficult to design a load line that intersected the same contour at two points. The strength of the dips in the absorber section IV curve is related to the number of carriers generated in the absorbing section of the device. Since this is directly related to the number of photons absorbed, strong dips require strong absorption as a function of voltage in the absorbing section and many photons generated by the gain section.

As the load line is made steeper by decreasing the series resistance, it is possible to force the laser to operate in the negative resistance regime of the absorber section IV curves by choosing an appropriate bias voltage. It was observed by Lau et al. [64] that this caused the laser to self-pulsate its output as a result of an electrical interaction with the negative resistance.

These self-pulsations observed in the laser output are not necessarily linked to mode locking. The mechanism driving the oscillations does not inherently link modes in phase and hence the pulses are better described as Q-switched. The frequency of the oscillations is usually the relaxation oscillation frequency [66] of the diode laser since the driving mechanism is not frequency selective [67]. However, when mounted in an external cavity, self-pulsating lasers have been successfully mode locked [68]. In this case, the researchers observed that the shortest pulses (35 ps) were observed when the gain was biased just above the "light jump" of a self-pulsating laser.

The parameter space for these self-sustained oscillations often overlaps with the parameter space for mode locking [43]. This is a particularly important observation for mode locking at high repetition rates, where the simultaneous presence of self-pulsations presents a low frequency modulation of the pulse train, often seriously diminishing the magnitude of the mode locked pulses. A theoretical analysis has shown that self-pulsations occur when the unsaturated absorber losses are large and for unsaturated gain to loss ratios only somewhat larger than unity [69]. Thus, in order to suppress the self-pulsations the laser should have a relatively small amount of absorption and a significant ratio of unsaturated gain to loss. This places an upper limit on the absorber length allowable to avoid self-pulsations, which becomes particularly critical at high repetition rates [6].

In addition to the constraints imposed on the absorber length to suppress self-pulsations, there is an optimal absorber length for mode locking. The amount of pulse

shaping per pass increases as the amount of unsaturated absorption is increased, although this flattens out for very high levels of absorption [6]. At the same time, as the absorption increases, the gain required from the gain section increases, such that the improvements in pulse shaping may not be easily realizable due to the demands on the gain section. Thus there is an optimal regime where the amount of absorption results in significant pulse shaping without requiring excessive gain. This implies that a relatively low ratio of unsaturated gain to absorber loss is desirable for the shortest pulse widths. Thus, it is not surprising that the shortest mode locked pulses are often obtained at the boundary between self-pulsation and mode locking [69].

Relating these properties to the IV curves, the amount of unsaturated absorption decreases with shorter absorber sections and with increased applied absorber section voltage. Thus, a small absorbing section biased outside the negative resistance regime of the IV curves should provide self-pulsation free saturable absorption. The length of this section should then be optimized to achieve sufficient absorption to provide adequate pulse shaping.

4.2 The Effects of Biasing on Temporal Characteristics

The other important consideration in the design of a saturable absorber is its temporal characteristics. A saturable absorber can be characterized as fast or slow depending on whether its relaxation time is short or long relative to the pulse duration [70]. Semiconductor saturable absorbers used in mode locked lasers typically

have absorber recovery times in the tens to hundreds of picoseconds [6] whereas typical pulse widths are in the 1 ps regime. Therefore, semiconductors are considered to be "slow" saturable absorbers. This means that the pulse width is not limited by the recovery times of the gain and absorption so long as the absorber recovers faster than the gain and the absorber recovery time is less than the cavity round trip time [71].

The recovery time of unbiased semiconductor material is typically too slow to be used in mode locking at repetition rates above several GHz because the spontaneous emission lifetime is too long (about 1 ns) [6]. Although it is possible to increase the recovery rate with nonradiative recombination centers as discussed in chapter 2, it is preferable to remove the carriers using a reverse bias. Thus it is necessary to choose an absorber section bias voltage that provides an appropriate level of absorption while allowing a reasonably fast recovery time. Additionally, the resistance in series with the absorber section should be as small as possible to ensure the removal of carriers is not hampered by a large RC time constant.

4.3 Experimental Design for Multisegment IV Characterization

In order to characterize the split contact lasers, an experimental arrangement was designed that would automatically adjust and simultaneously measure the IV curves for both the gain and absorber sections while recording the light emitted from each laser facet. This makes it possible to efficiently and accurately obtain curves from which one might be able to predict the optimal biasing conditions for mode locked operation.

The lasers were mounted on the same test station as described in chapter 3. The only difference was the use of a second probe to make contact to the second section of the laser. The gain section of the laser was driven by the ILX laser driver. The current and voltage for this section were recorded on a computer over the GPIB bus.

Since it was necessary to obtain IV curves for the absorber section as a function of gain section biasing, it was preferable to bias the absorber section with a voltage source controllable by the computer. Since most laser drivers are unable to operate as a programmable voltage source, electronics were designed as shown in figure 4.3. This consisted of an 8 bit DA converter connected to the digital I/O port of the data acquisition card in the computer (RTD AD3300). The output from the DAC was modified to give the optimum voltage range and offset, so as to drive the lasers over a reasonable biasing region. These parameters were designed to be easily adjustable so that lasers with different characteristics could be easily tested. In order to source enough current for the lasers, the output stage was a power opamp chip (LM759) capable of sourcing as much as 250 mA. The output voltage and a voltage proportional to current through the diode were measured by the computer, and software was written to automate the entire measurement and adjustment cycle.

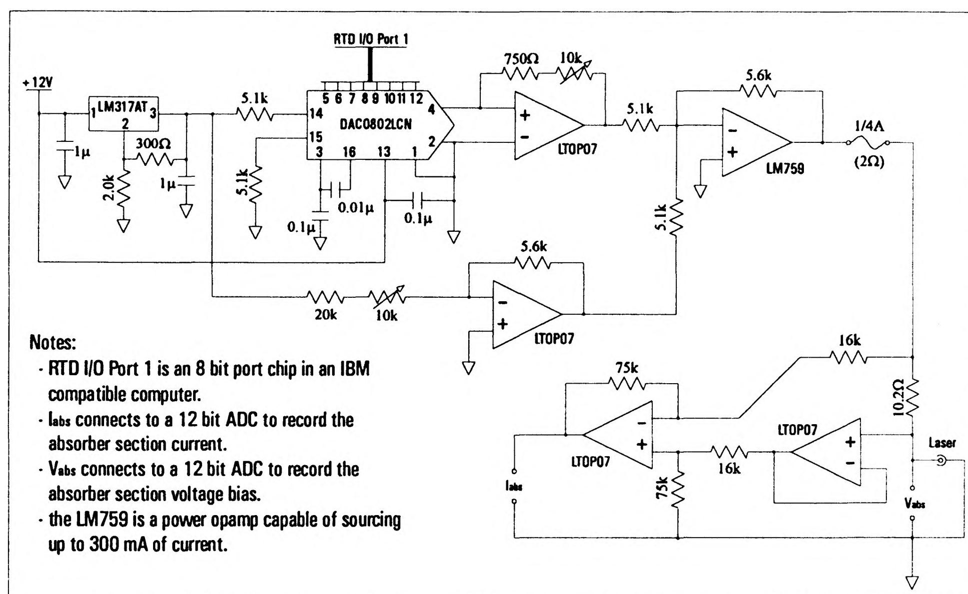

Figure 4.3: Programmable voltage source for absorber section biasing.

4.4 Results from Split Contact Characterization

Split contact laser bars were cleaved for each of the laser types discussed in chapter 3. Multiple lasers on each bar were tested in order to identify "dips" in the IV curves of the absorber section. Dips were not observed for either the 850 nm lasers or the 980 nm lasers from growth 2391. In each case, the most reasonable explanation for this was that there was not enough light produced to create enough photocurrent in the absorber section to dominate a portion of the IV curve. In the case of the 850 nm lasers, this was because they did not lase until the current was greater than 50 mA. With an absorption section, a larger pump current would be required for the laser to overcome the increased losses and reach threshold. These lasers were unable to operate under these conditions for a long enough period of time for multiple IV curves to be measured. The

980 nm lasers failed immediately under the pumping requirements necessary to obtain absorbing section IV curves.

Fortunately, the existing SQW 980 nm lasers do work reliably and were therefore used to test the functioning of the electronics and software. In addition, their similarities to the new laser designs made it possible to draw some conclusions in terms of the geometrical properties of an ideally designed device. In order to do this, three 1200 μm laser bars were cleaved from the same region of a quarter wafer. The sizes of the contacts were varied for the three bars so as to potentially observe any trends that would lead one to be able to recognize a preferable absorber to gain section ratio for a desirable set of characteristic IV curves. A diagram of the geometry of these lasers is shown in figure 4.4.

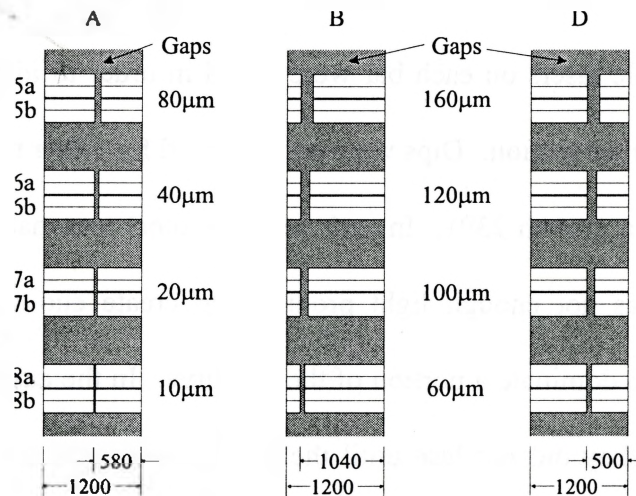

Figure 4.4: Geometry of the split contact lasers tested (all dimensions in μm).

The other geometrical issue that was of concern was to find an ideal gap width. Given a set doping level, as the gap between contacts is widened, the resistance increases. A higher resistance between contacts should reduce electrical leakage between the two

sections of a device. However, a wider gap also results in inferior optical coupling between sections, which is undesirable. The mask used to process a quarter wafer has a mixture of gap widths that are organized such that there are two gap series: large and small. Each series of gaps consists of four widths that increment in a pattern such that there is a laser pair for each gap width for the 3 μm and 4 μm ridges. This makes it possible to compare the properties of several lasers on the same bar with different gaps but otherwise similar absorber and gain sections. In this way, the same ridge width is used for all tests, thereby avoiding the complication of different laser characteristics unrelated to the contact geometry.

By comparing the IV curves, it is possible to draw some useful conclusions about how one should design a saturable absorber section. For laser bar A, the IV curves are shown for four lasers in figures 4.5(a) through 4.5(d). All of these lasers have 3 μm wide ridges and 620 μm long gain sections. The absorbing sections ranged from 570 μm to 500 μm long depending on the gap width. The plots are arranged in order of decreasing gap widths. Clearly, the dips are larger for shorter gaps. This indicates that the light emitted from the gain section is heavily absorbed within a short distance in the absorber section.

The resistance values for these gaps were 1020 Ω, 949 Ω, 921 Ω, and 903 Ω respectively. These resistances are quite similar, and not surprisingly the leakage current from the gain section is small, as is evidenced in the graphs. Clearly, reducing the width of the gap has a very large effect on the split contact performance of the device at the

expense of only reducing the gap resistance slightly. This indicates that using the smallest gaps on the mask is preferable for these lasers.

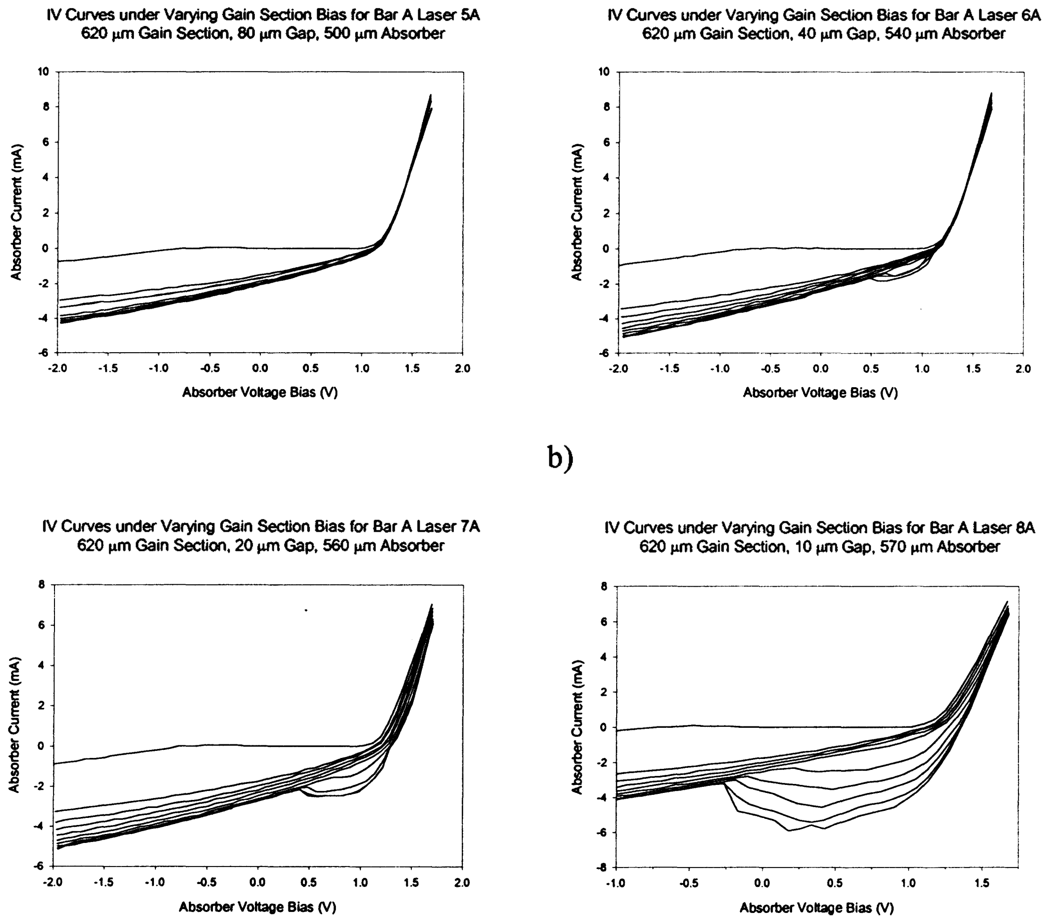

c) d)

Figure 4.5: IV curves for four split contact lasers with different gap widths for varying gain section biases. a) Laser 5a: 80 μm, b) Laser 6a: 40 μm, c) Laser 7a: 20 μm, d) Laser 8a: 10 μm. In each case, the traces step from 0 mA to 45 mA in 5 mA increments.

In order to determine the effect of varying the contact dimensions, it is again instructive to compare the absorber section IV curves. These are shown in figure 4.6(a) through 4.6(d). The data suggest that light generated by the gain section is heavily

absorbed within a short distance in the absorber section. For the devices tested, decreasing the absorber section length resulted in larger dips. One would expect that this trend would be reversed for exceedingly short sections, where only a small fraction of the photons generated in the gain section were absorbed in the absorbing section. Thus one can conclude that very small gaps are preferable for mode locking applications, as this allows sufficient absorption to be obtained while negatively biasing the absorber section to sweep out carriers, thereby shortening the absorber recovery time.

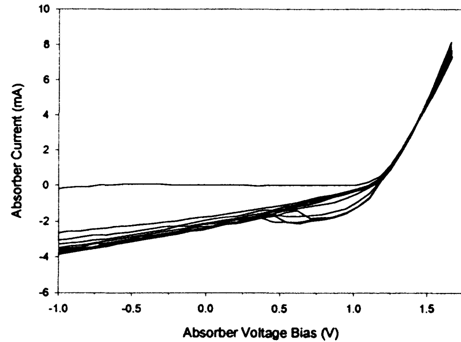

a)

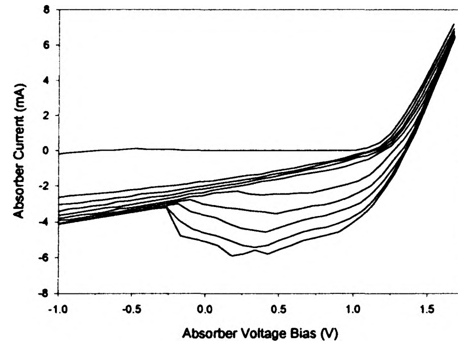

b)

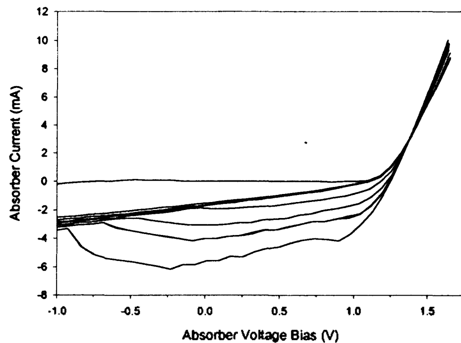

c)

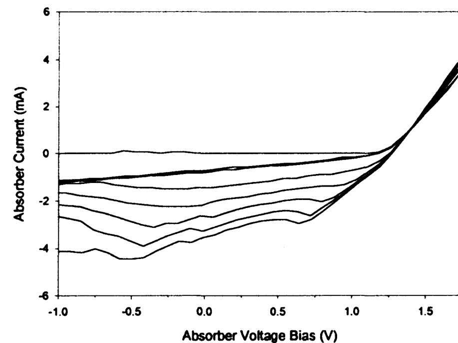

d)

Figure 4.6: IV curves for four split contact lasers with different gain section / absorber section ratios for varying gain section biases. a) Bar A laser 8a: 570 μm / 620 μm, b) Bar A laser 8a: 620 μm / 570 μm, c) Bar D laser 8a: 700 μm / 440 μm, d) Bar B laser 8a: 980 μm / 160 μm. In each case, the traces step from 0 mA to 45 mA in 5 mA increments.

Chapter 5: Antireflection Coatings

The design and fabrication of antireflection (AR) coatings is of great importance to the operation of external cavity diode lasers. The simplest external cavity consists of only a lens and a mirror feeding light back into the facet of the laser. Due to the diode laser's relatively low bare facet reflectivity, significant amounts of light can be coupled back into the laser. However, if the facet is not AR coated, the amount of feedback is reduced and the two Fabry-Perot cavities become strongly coupled. This is not desirable for a mode locked laser, as the short cavity usually produces a pulse train of spikes superimposed on the desired pulse train generated by the longer external cavity. This causes the peak power for each of the external cavity pulses to be greatly reduced. These coupled cavity effects must be overcome by reducing the reflectivity of the facet through which light will be fed back.

There are at least two ways to achieve suitably low reflectivity facets: antireflection coatings and angled facets. Angled facets reduce the Fabry-Perot cavity reflectivity by causing reflections to be diverted from the waveguide, while AR coatings use interference filters to eliminate on-axis reflections. Angled facets introduce additional complications in the laser processing stage and generally show improved performance only if they are additionally AR coated [72]. Hence, at the present stage of this project, angled facets have not been investigated. However, they will eventually be

studied as this project matures, as a means to improve the performance of external cavities and semiconductor optical amplifiers.

The quality of the antireflection coating is critical to achieving short, single pulses from diode lasers in external cavities. Many researchers have quoted that the residual facet reflectivity should be maintained below 10^{-4} in order to reduce coupled cavity effects to an acceptable level [13, 14, 15]. The tolerances required for the index and thickness control of the deposition system represent a significant technical challenge. As a result, this is an ongoing area of research. However, films with residual reflectivities in the low 10^{-4} range have been previously deposited on semiconductor substrates using the McMaster ECR-CVD system [73]. Further investigations of the deposition and characterization of such coatings on laser facets will be discussed in this chapter.

5.1 Thin Film Deposition using ECR-CVD

An electron cyclotron resonance chemical vapour deposition (ECR-CVD) system uses a plasma to crack the precursor gas in order to deposit the desired material on a substrate. The primary advantage of ECR-CVD over other deposition systems for semiconductor applications is that the velocity of the ions and reactive species impinging on the sample can be controlled by the magnet design such that the energies are small enough to avoid damaging the sample [74]. This is an important consideration for a laser facet composed of InGaAsP layers, since these materials are particularly sensitive to damage and to elevated temperatures, where excessive heating can result in the loss of

group V elements. Additionally, if point defects are introduced through ion bombardment [75], they could result in local centers of heating which could cause deterioration of the laser performance and eventually lead to premature failure.

A schematic diagram of our ECR-CVD system is shown in figure 5.1. Microwave power generated by the magnetron head is introduced into the top of the plasma generation chamber through a quartz window. Stub tuners, positioned along the waveguide, are used to impedance match the waveguide system in order to optimize the power coupled into the plasma by reducing the reflected power.

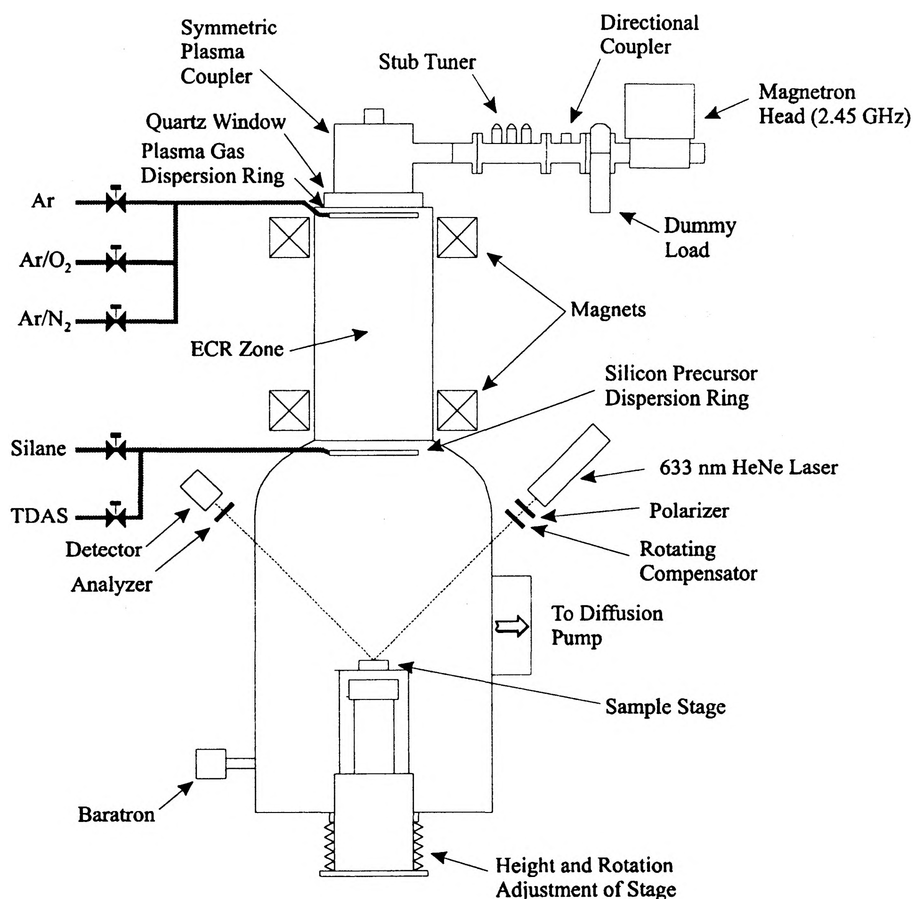

Figure 5.1: The McMaster ECR-CVD system.

Two large electromagnets are positioned around the upper half of the deposition chamber. The plasma gases (Ar, O_2, and N_2) are introduced through a dispersion ring at the top of the deposition chamber. When the magnets and microwave power are on, the electrons in the plasma experience a Lorentz force proportional to the electric and magnetic fields applied:

$$\mathbf{F}=q(\mathbf{E}+\mathbf{v}\times\mathbf{B}). \quad (5.1)$$

The magnetic component causes the electrons to follow a helical path with a cyclotron frequency of

$$\omega_c = eB/m_e \quad (5.2)$$

and a radius defined by conservation of energy. By tuning the magnetic field so that the cyclotron frequency matches the microwave frequency, a resonant condition exists where the electrons continuously gain energy from the electric field. The region where this holds is referred to as the ECR zone. As the electrons gain energy, the radii of their helixes increase, thereby increasing the probability of collisions with other bodies in the plasma. Eventually, a state of dynamic equilibrium is reached where there is a balance of energy gained from the electric field and energy lost through collisions. For our ECR-CVD system, the microwave frequency used is 2.45 GHz, so the corresponding magnetic field strength required to satisfy the resonant condition is 875 G.

The silicon precursor is introduced through a dispersion ring located below the lower magnet. The Ar, O, and N ions leaving the plasma collide with the precursor gas molecules, breaking them into various radical species which may react with one another

at the sample surface, depositing a film on the sample in the sample holder. Waste products are removed from the system using a diffusion pump.

The precursors used in this system are tris-dimethylamino silane (TDAS) and silane. The chemical structures for these are shown in figure 5.2. Silane, is the more commonly used precursor in industry, however, extensive work has been done using TDAS in our system because it is a safer alternative [76]. Recently, studies have been performed to compare and contrast the deposition properties of silane and TDAS [77]. Because of the nitrogen content in TDAS, it is not suitable for depositing the highest index (amorphous silicon) films. Therefore all of the coatings deposited in this thesis were made using silane.

Silane:

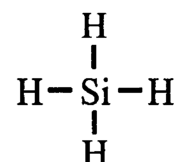

TDAS:

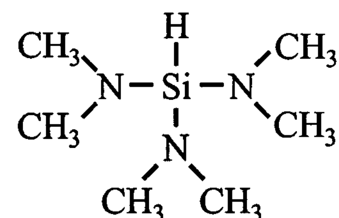

Figure 5.2: The silicon precursors.

Samples are mounted on a sample holder which is brought into the deposition chamber via a load lock (not shown in the diagram). The sample holder is then placed on a heated stage in the deposition chamber. The sample temperature is monitored using a thermocouple placed in contact with the top of the sample. Lasers were mounted as shown in figure 5.3. The laser bar was held in place by weak horizontal pressure from the two pieces of silicon clipped to a silicon wafer mounted on the sample stage. The silicon wafer was used to reduce the possibility of damage to the uncoated laser diode facet, which would otherwise rest directly on the steel sample stage. For a 500 μm wide laser

bar, the pieces of silicon used to clamp it in place were chosen to be 300 μm and 700 μm so that the electrical contacts would be satisfactorily masked during the deposition. The active region was closest to the 300 μm piece so as to avoid possible shadowing effects from the 700 μm piece of silicon.

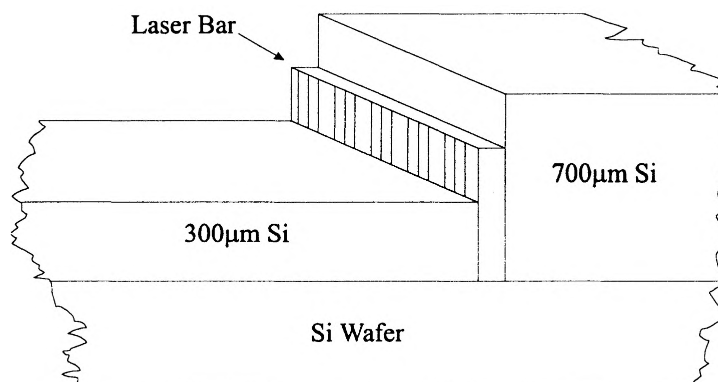

Figure 5.3: Mounting a laser bar for a deposition.

The index and thickness of the films are monitored in real time using a computer controlled in situ ellipsometer operating at 633 nm. Software converts the ellipsometric data to estimations of index and thickness based on a standard model. For a single layer coating, this is quite accurate. However, as the number of layers deposited increases the accuracy of the predicted index and thickness for the current layer decreases dramatically. This is because the software must base its calculation on the previous layer's index and thickness, thereby accumulating the uncertainties of previous calculations. Therefore, it is preferable to measure the first layer of each composition to be deposited and the time required to grow the layer. Subsequent layers can then be timed using the growth rates of the first layers. This assumes that the composition of different layers grown with the same gas flow rates are approximately the same.

The system is currently used exclusively to deposit silicon oxynitride thin films. These films vary in composition from amorphous silicon to Si_3N_4 to SiO_2. This allows the index of refraction of the films to range from 3.5 to 1.9 to 1.5 respectively. Calibrations have been performed so that the flow rate can be set during a deposition to obtain a composition with a desired index of refraction.

5.2 Antireflection Coating Design

An antireflective coating works on the principle of creating an "optical impedance match" between the air and the substrate. Light arriving at the different layers of the interface is reflected such that the exiting wavefronts are out of phase with one another. Thus they add destructively, and the reflected intensity is effectively zero at the design wavelength.

The simplest antireflection coating is a single layer film, a quarter of a wavelength thick, made out of a material that has an index of refraction that is equal to the square root of the products of the indices of the substrate and air:

$$n = \sqrt{n_0 n_s}\ . \tag{5.3}$$

The thickness of the coating designed to be perfectly antireflecting at a wavelength λ is then

$$t = \lambda/4n\ . \tag{5.4}$$

An ideal filter designed for 980 nm has a wavelength response as shown by the solid line in figure 5.4.

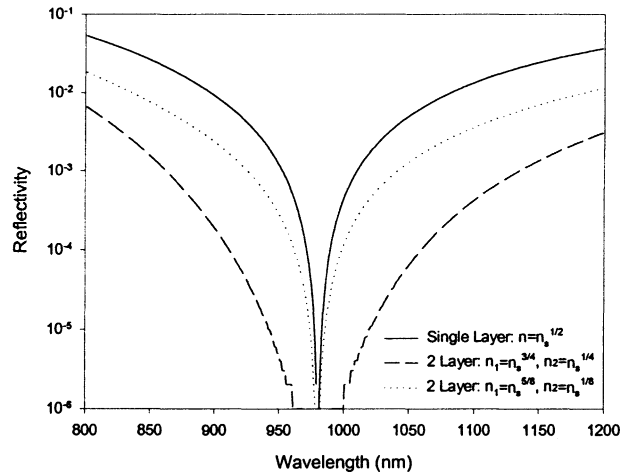

Figure 5.4: Comparison of single layer and two layer AR designs for 980 nm on a substrate with n=3.6.

The notch can be broadened by depositing a multilayer stack of dielectric materials [78, 79]. In this case, the index of refraction of each layer is determined by considering each layer as an optical impedance match between the adjacent layers. A general expression for the layer index of refraction constraints for an AR stack with k quarter wavelength layers that reaches zero reflectivity, as obtained from matrix methods, is then:

$$\text{If k is even:} \quad \frac{n_s}{n_0} = \left(\frac{n_2 n_4 n_6 \ldots n_k}{n_1 n_3 n_5 \ldots n_{k-1}} \right)^2 \tag{5.5}$$

$$\text{If k is odd:} \quad \frac{n_s}{n_0} = \left(\frac{n_1 n_3 n_5 \ldots n_k}{n_2 n_4 \ldots n_{k-1}} \right)^2 . \tag{5.6}$$

These constraints still provide many possible solutions that reach zero reflectivity. However, different ratios of n's that satisfy the above constraints give different

reflectivity profiles. To demonstrate this, the reflectivity profile of two 2 layer antireflection coatings designed for 980 nm were calculated assuming a substrate index of 3.6. The results are shown in figure 5.4 and contrasted with the reflectivity profile for an optimal single layer film (solid line). Assuming $n_0=1$, for a 2 layer coating, $n_2/n_1=n_s^{1/2}$, so there are many solutions that satisfy this. The dashed line represents the reflectivity for $n_2=n_s^{3/4}$ and $n_1=n_s^{1/4}$ which represents the optimal width design [78]. The dotted line corresponds to $n_2=n_s^{5/8}$ and $n_1=n_s^{1/8}$. Clearly this has a narrower response than the optimal width design while still being wider than the single layer design. One can think of a single layer design as an extreme case of a two layer design where the "second" layer is air ($n=n_0$).

All of the preceding theory assumes that the interface is illuminated with plane wave light. Although this is very useful information when designing antireflective coatings for many macroscopic optical components, the predictions fall short when such coatings are applied to laser diode facets. The reason for this is that the light emanating from the facet of a laser diode is produced within a narrow waveguide such that the exiting beam diverges significantly. Hence, the wavefronts are not planar and the waveguiding properties of the laser must be taken into account.

To a very good first approximation, this is done by considering the active region of the laser to be a slab waveguide. A rigorous mathematical model was developed by Vassallo [80, 81] to model the modal reflectivity of a facet of a slab waveguide. Software has been developed previously to implement a simpler numerical approximation to the

rigorous model [82]. A comparison of the results of the two calculations indicates that the approximation is in very good agreement with the rigorous model in the limit of moderate to weak waveguiding [80].

The optimization section of the code was modified slightly in order to improve the efficiency of arriving at the new optimum coating parameters and to ensure the accuracy of the final design. The approach taken was to start the optimization code from the waveguide effective index computed for the laser design (as discussed in section 3.1). The error between the logs of the reflectivities of the modal and target designs is then minimized by adjusting the filter parameters. This is computed for a fairly large number of points (typically 40) over a broad wavelength range in order to obtain a broadly accurate filter. The resulting design can then be tested over a narrower region close to the center wavelength in order to fine tune the design if necessary.

This program was used to design single layer AR coatings for both of the 980 nm lasers and the 850 nm laser. The results are shown in figures 5.5 through 5.7 respectively. In each plot, the solid line is the reflectivity of the filter obtained by the plane wave design, deposited on a substrate with an index of refraction corresponding to that of the laser's active region. The dotted line is the reflectivity that would be obtained if that coating were to be deposited on a laser facet. Clearly, in each case, the center of the notch of each dotted line is not at the desired wavelength. Additionally, the minimum reflectivities are not low enough to be adequate for use in an external cavity laser design. The dashed line in each plot represents the theoretical reflectivity curve for a filter

accounting for the modal reflectivity, deposited on the laser facet. This curve is hard to distinguish from the target plane wave design, as there is very little error after the optimization.

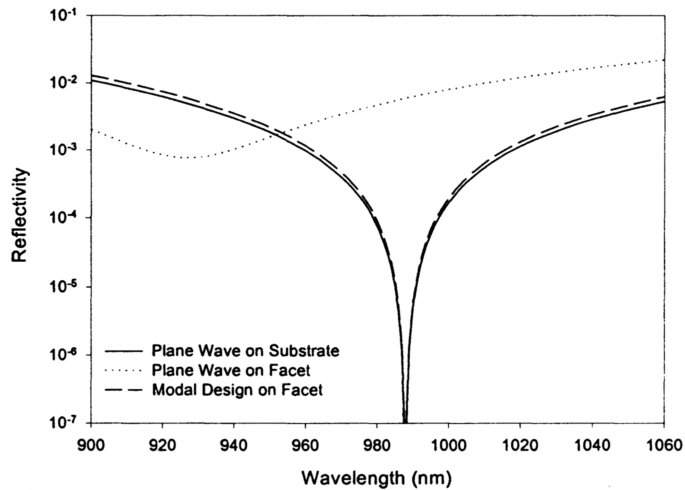

Figure 5.5: Comparison of AR designs for the existing SQW 980 nm laser design (988 nm).

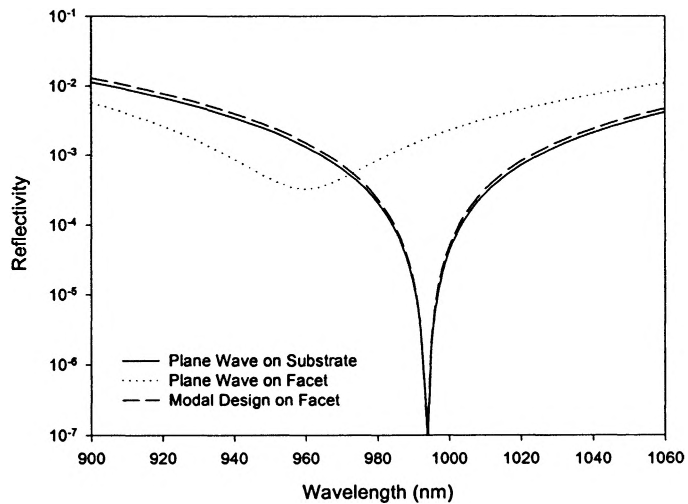

Figure 5.6: Comparison of AR designs for lasers processed from growth 2391 (994 nm).

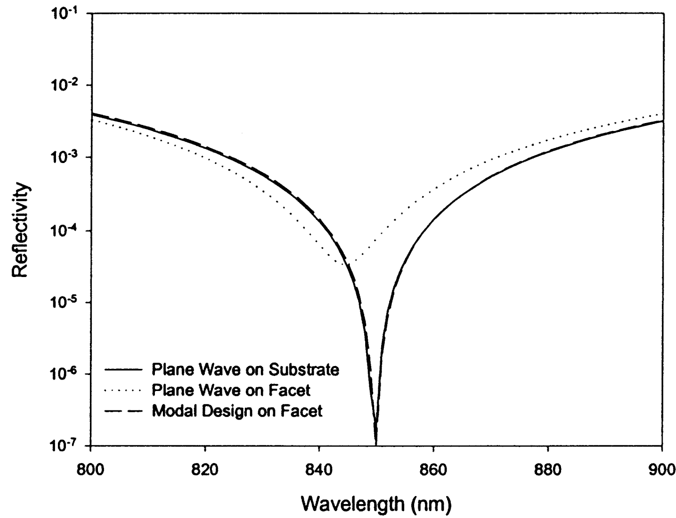

Figure 5.7: Comparison of AR designs for lasers processed from growth 2486 (850 nm).

	SQW 980 nm	980 nm Laser	850 nm Laser
Wavelength	988 nm	994 nm	850 nm
Plane Wave Design n	1.877	1.854	1.828
Plane Wave Design t	1316 Å	1340 Å	1162 Å
Modal Design n	1.854	1.824	1.818
Modal Design t	1424 Å	1412 Å	1176 Å

Table 5.1: Specification of AR coating parameters for the plane wave and modal designs given for each laser.

All deposition systems have some uncertainty in the characteristics of the films they produce. A conservative estimate of the run to run repeatability of our system would suggest a film could be deposited with an index uncertainty of ±0.005 and a thickness uncertainty of ±7 Å. An estimate of the effect of growing films at either end of these tolerances was made for the new 980 nm laser design. The results are shown in figure

5.8. The solid line is the optimal coating design while the dashed lines indicate the maximum response deviation expected from the above tolerances. Clearly there is a combination of a shallower notch and a shift in its center wavelength, the combination of which produces an inferior AR coating at the target wavelength. However, for comparison purposes, the plane wave design's response on the facet clearly shows that even with some uncertainty in n and t, the modal reflectivity design is preferable.

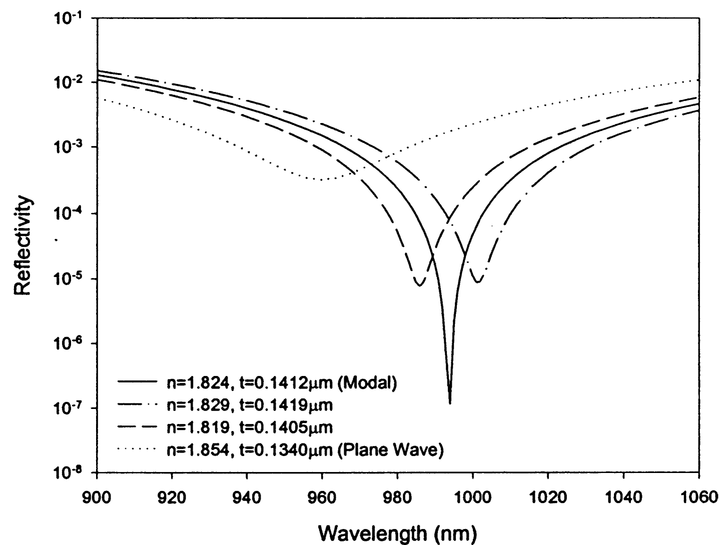

Figure 5.8: Estimation of uncertainty introduced into the film reflectivity profile due to deposition system tolerances.

5.3 Characterization of AR Coatings

Once a coating has been deposited, its performance should be quantified. There are many materials characterization techniques that are relevant to understanding the quality of thin films deposited in such a system. However, for an AR coating, it is most

important to characterize the reflectivity as a function of wavelength. The most straightforward way to measure the broadband reflectivity of a film deposited on a substrate is to mount it so that it can be scanned in a spectrophotometer.

In order to make the spectrophotometer measurements, it was necessary to use an adapting mount, which consisted of two gold coated prisms and a mirror mount on which the sample was affixed as described in reference [82]. This was mounted in the path of one of the beams of the spectrophotometer so that the transmittance read by the instrument was actually the reflectance of the sample. Since the instrument used was a double beam spectrophotometer, it compensated for spectral variation in the source and detector. However, it was essential to measure a known sample in order to take into account the absorbance of the gold coatings on the prisms and slight misalignments of the optical path.

The biggest problem associated with using a spectrophotometer to measure the films in this way is that a well-made AR coating's reflectance becomes so low near the notch in its reflectivity profile that the measured signal falls well below the noise floor of the instrument (approximately 10^{-3} reflectivity). It is then difficult to obtain a good estimate of the lowest reflectivity, which is of great importance. Therefore, a tunable diode laser based on a Littman-Metcalfe external cavity is frequently used to produce an intense light source that can be scanned over a narrow region (about 20 nm) at the notch of the filter response. The laser is ideal for this application since it is highly monochromatic, widely tunable, and reasonably powerful. The reflected light is then

measured using a silicon photodiode. We estimate that this method of measuring the reflectivity would easily be able to detect residual reflectivities as low as 10^{-6}.

5.4 Characterization of Modal Reflectivity

The previously described techniques are used to accurately measure the plane wave reflectivity of a film on a sample, and this is very useful for diagnostic purposes. However, in order to determine the reflectivity of a coating deposited on a laser facet as seen by the guided light, one must take a different approach based on the theory of laser diode operation.

When a diode laser operates below threshold, its broad spectral profile is modulated by a series of peaks and valleys corresponding to the Fabry-Perot cavity modes generated by the facets. The modulation depth of these structures is a function of the facet reflectivities of the laser under study. The steady state output intensity can be shown to be [83],

$$I^{\pm}(\nu) = \frac{B(1 + R_{\mp}G)(1 - R_{\pm})}{(1 + RG)^2 - 4RG\sin^2\theta} \tag{5.7}$$

This expression contains three unknown quantities: the reflectivities (R^2=R_+R_-), the gain (G), and the spontaneous emission factor (B). The latter can be eliminated by instead calculating the ratio of the maximum to minimum intensity for a given mode (corresponding to sinθ=0 and 1). When rearranged, this gives,

$$h = \frac{maximum}{minimum} = \frac{(1 + RG)^2}{(1 - RG)^2} \tag{5.8}$$

or, isolating the RG product,

$$RG = \frac{\sqrt{h} - 1}{\sqrt{h} + 1}. \tag{5.9}$$

Thus the product of the facet reflectivities and the gain can be determined for each mode by measuring the peak-to-dip ratio for the Fabry-Perot modulations in the laser's subthreshold emission spectrum. This is referred to as the Hakki and Paoli method [84, 85, 86]. If the RG product is measured before and after coating at the same pump current, G can be eliminated such that the change in reflectivity resulting from coating the laser can be determined [87, 88].

The problem with this method is that it assumes that one can very accurately measure the peak-to-dip ratio. Unfortunately, the recorded modulation depth is frequently reduced because the measured signal represents the true laser spectrum convolved with the instrument response function. Cassidy [83] showed that by integrating equation (5.7) over one free spectral range, and using the result to form a ratio with the minimum value of a dip, a more accurate measurement of the true gain is obtained. The ratio is then,

$$p' = \frac{\text{mode integral}}{\text{minimum}} = \frac{c}{2l}\frac{1 + RG}{1 - RG} \tag{5.10}$$

or, isolating the RG product,

$$RG = \frac{p - 1}{p + 1} \tag{5.11}$$

where $p = p'2l/c$ is effectively the "mode average" to minimum ratio.

Again, the Cassidy method can be used to determine the reflectivity of an AR coating by measuring the RG product before and after coating. Software was written to analyze data using both of these methods and compare the results.

Typically, the laser spectra are measured with a monochromator and photomultiplier configuration. For convenience, the light emitted by the laser was coupled into an optical fiber which was connected to an HP optical spectrum analyzer. This instrument is in essence a double pass monochromator with a calibrated detector and convenient data acquisition capability. It has a resolution of 0.1 nm on the smallest practical slit setting, which is sufficient to resolve the Fabry-Perot modes of a diode laser.

5.5 Single Layer AR Coatings on Laser Facets

In order to demonstrate our capabilities in depositing an AR coating on a laser facet while simultaneously showing the validity of the modal reflectivity model and the code used, two coatings were deposited on the 980 nm lasers from growth 2391. The first coating was intended to be the optimal AR coating designed using the modal reflectivity calculations. The target parameters for this coating were n=1.824 and t=1412 Å. The second coating was intended to be the optimal plane wave coating design that assumes the active region has an index of refraction of 3.438. The target parameters for that deposition were n=1.854 and t=1340 Å.

Based on readings from the in situ ellipsometer, the index and thickness as calculated for the first deposition were relatively close to the target values (n=1.836,

t=1401 Å). The index measured by the ellipsometer for the second coating decreased continuously as deposition progressed. Since the measured index at the half order (where Δ typically passes through a 360° to 0° transition) was much lower than intended, the deposition target thickness was recalculated during the deposition to give a quarter wavelength thick layer at the measured index (n=1.832, t=1356 Å).

The reflectivity profiles of the films deposited on the silicon witness samples were measured using the spectrophotometer. The experimental plots compared with the theoretical plane wave response of these films as deposited on silicon are shown in figures 5.9 and 5.10. Clearly the AR filter accounting for the modal reflectivity is centered at the same wavelength as the theoretical plot. The plane wave model and experimental results are in greater disagreement, but this is likely attributable to the shift in the index of refraction during the deposition.

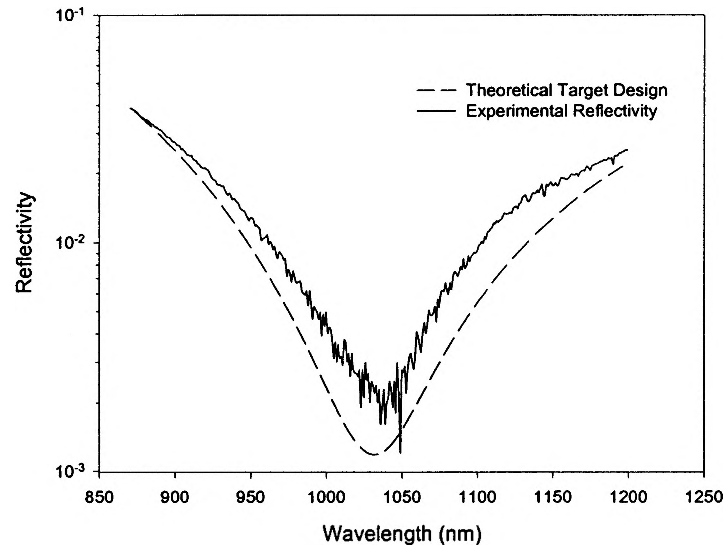

Figure 5.9: Reflectivity profile for the AR coating accounting for modal reflectivity as deposited on the silicon witness sample.

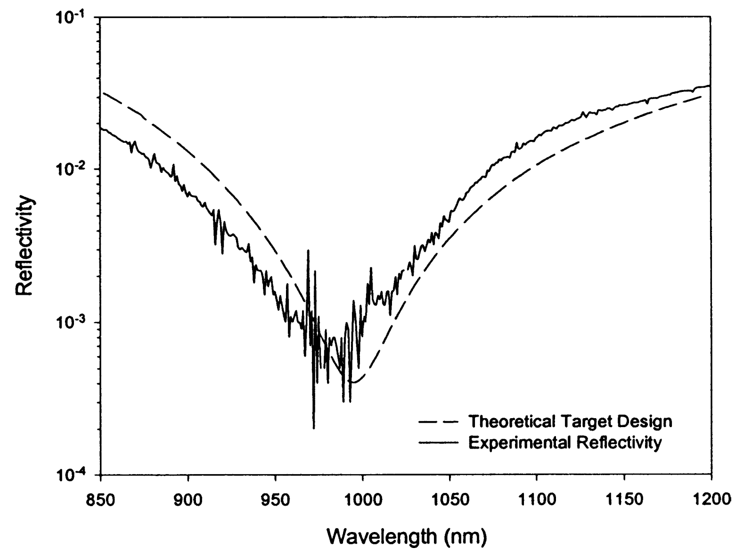

Figure 5.10: Reflectivity profile for the AR coating based on the plane wave model as deposited on a silicon witness sample.

The spectral responses for numerous lasers were measured for each bar at a variety of injection currents before and after coating. An example of the effect of the coating on the spectral response of the laser with identical pump currents can be seen in figure 5.11. Although there is a significant difference in the modulation depth of the Fabry-Perot modes in the two plots, the difference before and after coating is not as great as one might have expected.

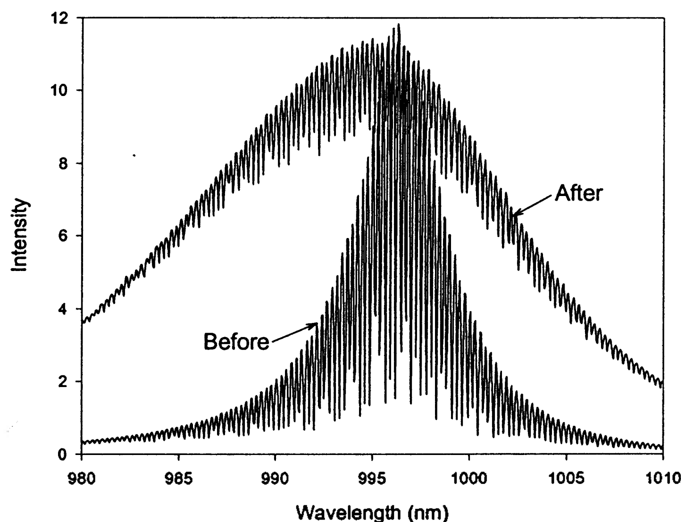

Figure 5.11: Comparison of spectra before and after coating laser 10b with the modal reflectivity AR design. The amplitude of the intensity scale is arbitrary and different for the two curves - the peak power of the before curve being much larger.

The modal reflectivity for the coated lasers was determined using both the Hakki/Paoli and Cassidy methods. Software was written to identify peaks and valleys and compute the RG product as a function of wavelength (corresponding to mode

numbers). Because there was noise superimposed on the data, it was necessary to prefilter the data such that the software would be able to accurately identify peaks and valleys. This was accomplished using a second order Butterworth digital filter, where the cut off frequency was adjusted to remove the noise and quantization while minimally altering the Fabry-Perot modulations. Although a Butterworth filter is not linear phase, and thus introduces some phase shift in the passband, the frequency of the noise components were of significantly higher "frequency" than the Fabry-Perot modulations, so the modes were typically shifted by less than 5 to 10% of a mode spacing.

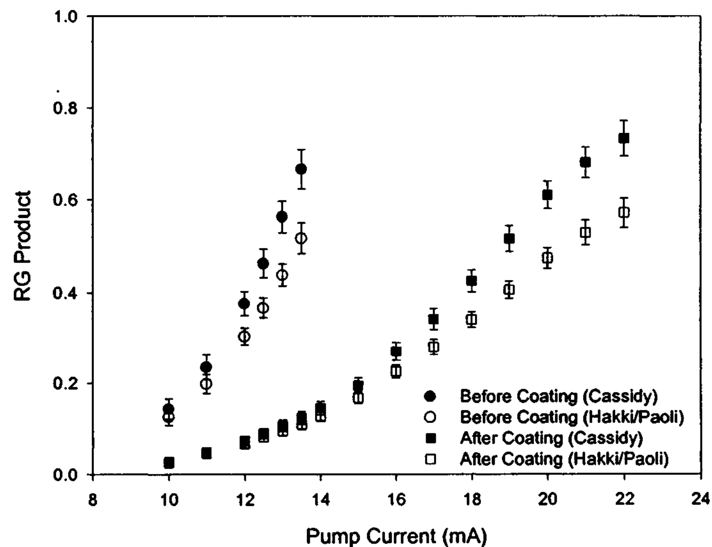

Figure 5.12: Comparison of average RG products before and after AR coating laser 12b with the film accounting for modal reflectivity.

Figure 5.12 shows the RG curves for laser 12b from bar G before and after coating the laser facet with the AR coating that accounted for the laser's modal

reflectivity. Clearly the AR coating reduced the RG product. However, the reflectivity calculated from this was 6%, which was significantly higher than expected.

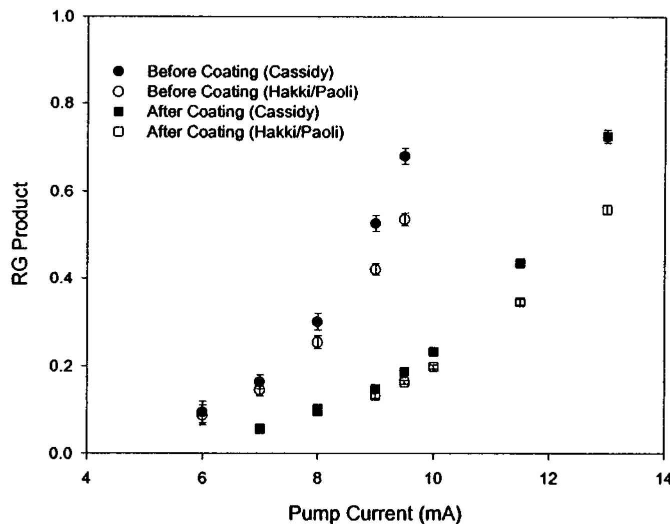

Figure 5.13: Comparison of average RG products before and after AR coating laser 9b with the plane wave filter.

In contrast, figure 5.13 shows the RG curves for laser 9b from bar F before and after coating with the plane wave filter. Once again, the AR coating has reduced the RG product, but not as much as the AR coating based on the modal reflectivity. The calculated reflectivity is approximately 9%.

The discrepancies between the measured facet reflectivities and those predicted by the model are significant. At the same time, the discrepancies for the plane wave results and theory are much smaller. The accuracy of the facet reflectivity measurements were later confirmed from measurements of the front to rear facet power ratio (as discussed in section 5.5). Thus an explanation for the variation in the results is needed.

The agreement between the theory and experiment for the coatings on silicon substrates implies that the index and thickness for the plane wave coating were close to the target values. One can therefore conclude that the index of refraction for the facet coating was also close to the target value. This leaves two possibilities: uncertainty in the active region index of refraction and variation in the film thickness on the laser facet as compared to the silicon substrates. A variation of ±0.02 in the index of refraction of the waveguide core resulted in a small shift in the center frequency in the model. The predicted residual reflectivity was still below 10^{-3} at 980 nm. Thus it was necessary to consider thickness variations as the source of the high facet reflectivities. By adjusting the thickness in the model, it was found that a thickness reduction of approximately 200 Å resulted in a residual reflectivity of approximately 5%. Such a substantial reduction of thickness could possibly be explained by shadowing of the laser facet by the edge of the 700 μm thick piece of silicon wafer. Although this was not anticipated at the time of coating, to ensure that this is not a problem in the future, both of the silicon pieces used to clamp the laser bars should be slightly thinner than the laser length.

5.6 High Reflectance Coatings

If antireflecting coatings can be considered an "optical impedance match," high reflectance coatings are the antithesis: an "optical impedance mismatch." While an AR coating produces a smooth transition of index from air to the substrate, an ideal high reflector produces the most abrupt transition possible. To achieve this, a stack consisting

of alternating high and low index of refraction quarter wave layers is deposited. The reflected wavefronts are in phase at the design wavelength so that they add constructively. The more layers that are deposited, the higher the reflectivity is at the peak. The higher the index contrast is between layers, the wider the central high reflectance band.

Such films have been grown in the ECR-CVD system by alternating between gas flows for the growth of high and low index material. High reflectance films can be grown using either the Si_3N_4 or SiO_2 systems. However, typically SiO_2 is preferable because of the higher index contrast possible. An optimally large index contrast HR film's layers would alternate between SiO_2 with an index of 1.5 and a material with a very low oxygen content, such that the index is roughly 3.2. A small amount of oxygen is desirable in the higher index layers because the amorphous silicon coatings have not been of as good quality as compared to materials including some oxygen.

Multiple layer films grown with oxygen suffer from a memory effect where oxygen from a high oxygen content layer attaches to the walls of the chamber and is then present in significant quantities during a low oxygen layer. Since oxygen is very reactive (it takes only a small amount of oxygen to create significant oxygen content in the films), this causes the index contrast for subsequent layers to be poorer. One solution to this is to use the nitrogen system, since nitrogen is much less reactive and does not show a memory effect. The drawback to this is that the index contrast for nitrogen based films is poorer since Si_3N_4 has an index of refraction of 1.9.

To demonstrate our capability to produce high quality high reflectance coatings on laser facets, a four layer HR stack was deposited on a laser bar consisting of 980 nm lasers. The laser bar used was cleaved from a section of lasers processed the same day so as to ensure that the surface of the facet to be coated was as clean and as free of oxides as possible. The coating was designed to be highly reflecting at 980 nm, corresponding to the wavelength at which the lasers operated. The filter design is shown in table 5.2.

Layer	Target Index	Target Thickness
Air	1.00	
SiO_x ($x \approx 0$)	3.40	720 Å
SiO_2	1.48	1655 Å
SiO_x ($x \approx 0$)	3.40	720 Å
SiO_2	1.48	1655 Å
Silicon (Laser)	3.6	

Table 5.2: Specification of a four layer HR stack for 980 nm.

The films deposited on the witness sample substrates were characterized using the spectrophotometer as described previously. The results are shown in figure 5.14.

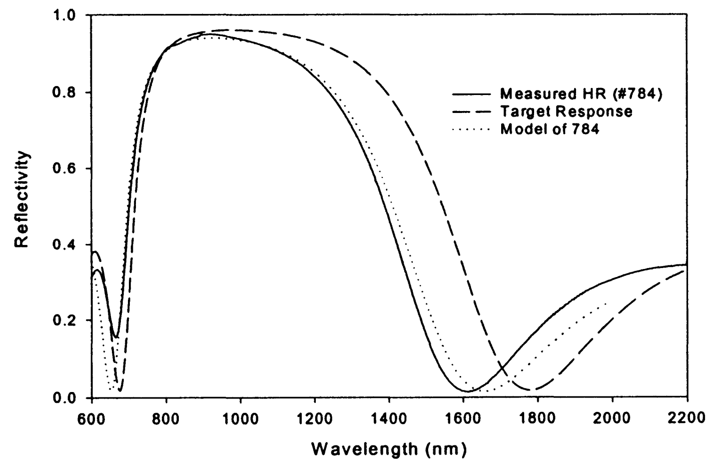

Figure 5.14: The reflectance profile of a four layer high reflectance stack deposited on an InP witness sample.

It is clear that the measured reflectivity profile (solid line) does not exactly match the target response (dashed line), although the reflectivities around 980 nm are similar. This discrepancy is likely due to the memory effects observed with oxygen, since the film is composed of alternating layers of high and low oxygen content starting with a high oxygen content film. To test this, the high index layer was reduced from 3.4 to 3.1 (dotted line), and the reflectivity profiles are indeed more closely matched. In reality, there may also be an additional contribution to the discrepancy due to uncertainty in the thickness deposited. Thus, although one can not necessarily conclude that the high index is exactly 3.1, it is clear that a lower index is the root of the difference.

Once again, the modal reflectivity profile at the laser facet is different from the plane wave design. Although it is possible to calculate an accurate modal reflectance profile for an HR coating as deposited on a laser facet, previous work [82] has shown that it is not necessary. Although many of the narrow bandwidth features shift in wavelength, the absolute reflectivity of the central, broad, high reflectivity region remains virtually unchanged. Since the modal reflectivity calculation for a multilayer stack is very time consuming to optimize, it is usually deemed sufficient to calculate the stack based on the plane wave model. As long as the broad central region is approximately centered on the laser's operating wavelength, any change due to the facet modal reflectivity will have a negligible impact on the laser's performance.

In order to confirm that the reflectivity of the HR stack deposited on the lasers matched the reflectivity of the coated witness samples, LI curves were measured for each

facet. Since the reflectivities of the facets are different, the light emitted by each facet should also be different. The ratio of the powers for the light emitted by the facets is related to the reflectivities by [82]:

$$\frac{P^+}{P^-} = \sqrt{\frac{R^-}{R^+}}\left(\frac{1-R^+}{1-R^-}\right). \tag{5.12}$$

If the reflectivity of one facet is known, then the reflectivity of the other facet can be calculated. The bare facet reflectivity can be estimated by calculating the normal incidence Fresnel reflectivity of an interface between the effective index of the laser waveguide and air:

$$R = \left[\frac{n_{eff}/n_0 - 1}{n_{eff}/n_0 + 1}\right]^2 = \left(\frac{n_{eff} - 1}{n_{eff} + 1}\right)^2. \tag{5.13}$$

The bare facet reflectivities were calculated to be 29.7% for the existing SQW 980 nm lasers, 29.3% for the 980 nm lasers from growth 2391, and 28.9% for the 850 nm lasers from growth 2486. The HR coated lasers were new 980 nm lasers, and the average reflectivity of the devices tested was determined to be 91.3% ± 3%.

Although high reflectance coatings are not our primary focus, there are many external cavity configurations that would benefit greatly from the application of HR coatings, some of which may be of interest to investigate in the future. One such example would be a fiber cavity where one end of the laser is AR coated to couple into a fiber and the other laser facet is HR coated to 95%. The fiber would incorporate a Bragg grating with a reflectivity somewhat less than 95% so that light would be emitted down the fiber.

Such a cavity design would be ideal for applications that would require fiber amplifiers or flexible positioning of the beam.

Chapter 6: Conclusions

In conclusion, the groundwork has been completed for a new research initiative on the generation of ultrashort pulses using mode locked diode lasers. Such lasers have wide ranging applications scientifically as well as industrially. In particular, several relatively unexplored applications involving multiphoton interactions would benefit from the development of moderate power ultrafast short wavelength diode lasers.

Although there are many ways to generate short optical pulses from diode lasers, mode locked devices are in general capable of producing the shortest pulses. Mode locked diode lasers can be driven actively, passively, or in combination, referred to as hybrid mode locking. This latter approach is of the greatest interest as it combines the pulse shortening aspects of passive mode locking with the timing stability of active mode locking.

In order to realize a hybrid mode locked diode laser system at repetition rates of interest, concurrent studies of a number of areas are necessary. These include the development of multisegment diode lasers and amplifiers, external cavities, AR and HR thin film coating of laser facets, and RF pulse generator development. In addition, the development of new short wavelength aluminum-free diode lasers is of particular relevance in multiphoton applications. The current status of the diode laser development,

split contact device characterization, and thin film interference filter development has been reported in this thesis.

6.1 Laser Designs

Two new short wavelength laser designs based on the InGaAsP/GaAs system have been realized with significant levels of success. Aluminum-free short wavelength lasers are of great interest due to their perceived improved long term reliability. Thus these new lasers, nominally emitting at 980 nm and 850 nm, are of particular relevance.

The lasers were developed based on the results of a computer model of a ridge waveguide structure. Reasonable qualitative correlation between the physical device model and the far field behaviour was observed, suggesting that this is an appropriate methodology for the development of new devices. In order to further improve the accuracy of the model predictions, future studies of the physical properties (primarily the index of refraction) of InGaAsP quaternaries lattice matched to GaAs would be highly appropriate.

After studying the properties of a previously developed GaAs waveguide 980 nm laser design, several issues were identified that would need to be addressed in the new laser designs. The most important of these were the large divergence of the far field of the laser and the somewhat low electrical isolation between contacts. A new 980 nm laser with improved beam properties was produced, incorporating these ideas. A quaternary waveguide region was used to reduce the index contrast of the waveguide and

an improved active region thickness was chosen based on results of the computer model. The electrical isolation between contacts was improved by reducing the thickness of the cladding region below the etch stop while simultaneously reducing its doping level. These lasers performed well, and other than a small unforseeable processing error that reduced the device lifetimes, satisfied the goals of the design.

The expertise gained from developing the materials for the 980 nm laser made it possible to grow a quaternary suitable for the waveguide surrounding GaAs quantum wells. Thus, an 850 nm laser was developed. These lasers had high thresholds and exhibited some unusual properties, but their far field performance was good. The unexpected emission of red light from the facets as well as the high thresholds can be explained by spinodal-like decomposition of the quaternary used as the barrier/waveguide region of these devices.

There are several areas that should be investigated in the future to further develop and improve aluminum-free short wavelength diode lasers. The first is to determine optimal growth parameters for InGaAsP quaternaries which are lattice matched to GaAs, in order to reduce the amount of spinodal composition encountered during the MBE growth. This would make it possible to improve the current designs as well as to develop other new short wavelength lasers. The next step in this direction would be to develop a shorter wavelength laser (such as 808 nm) composed of quaternary quantum wells as well as a quaternary waveguide.

In addition to improving the materials aspect of the lasers, long term designs would benefit from active regions optimized for high power and wide gain bandwidth. Higher powers can be achieved using somewhat larger waveguide cores along both axes. In addition, tapered or flared lateral waveguides could yield improved control over the waveguiding properties while optimizing the gain and absorber section saturation energy densities. A wider gain bandwidth is realizable using optimized staggered quantum wells combined with dielectric coatings designed to flatten the gain profile.

6.2 Split Contact Design and Characterization

Split contacts are a very effective and particularly flexible means to introduce a saturable absorbing element into a diode laser. By adjusting the absorbing section's biasing, it is possible to operate a split contact laser in numerous regimes such that effects ranging from normal CW lasing to LI curve hysteresis and self-pulsations are obtainable. All of these effects result from changes in the absorption properties of the device, and can be optimized by choosing appropriate absorber section lengths, gap widths, and biasing conditions for the laser.

In order to characterize these devices, electronics and computer software have been developed such that it is possible to simultaneously adjust and measure the IV curves and LI curves for both sections of a split contact diode laser. This test configuration has been used to characterize the properties of numerous split contact lasers

and arrive at conclusions regarding the optimal biasing conditions for such lasers as well as optimal device geometries in terms of split ratios and gap widths.

It has been determined that the gap width between sections should be as small as possible while still maintaining electrical isolation because the absorption coefficient for unpumped material is quite large. Hence few photons make it through a large gap to be collected in the absorbing section of the device. The net absorber section length should also be very short to ensure that the laser can be easily biased in a regime that is satisfactory as a saturable absorber for mode locking applications while eliminating self-pulsations at the resonance oscillation frequency. A very short section would have to be negatively biased to provide significant absorption. Under these circumstances, the absorber recovery time would be substantially reduced as carriers are rapidly swept out of the active region by the reverse bias. This is a necessity to sustain stable fast repetition rate mode locking.

Further studies of optimal absorber section length and gap width should be performed to more directly quantify the relationship between geometries and biasing with the pulse width of a passively mode locked laser. Although these issues have been studied for high repetition rate passive mode locking, there is not an abundance of this information available for lower repetition rates, and for various external cavity configurations. Such detailed investigations will be straightforward using the equipment developed once a functioning external cavity mode locked diode system is achieved.

6.3 Thin Film Interference Coatings

Antireflection coatings are critical to the performance of external cavity diode lasers as they are necessary to strengthen the coupling of the gain medium to the external cavity while reducing the coupling between the two cavities. This is particularly important in mode locked diode lasers where residual reflectivities below 10^{-4} are necessary to ensure the pulses produced do not have substructure.

Optimal single layer AR coatings were designed for all three laser designs, taking into account the modal reflectivity of the laser facet. As a comparison of the plane wave and modal AR coating performance, each was deposited on a laser facet as well as on silicon witness samples. The reflectivity profiles of the films deposited on silicon were measured and compared with theory with reasonably good agreement. The laser modal reflectivity was determined for each coating using the methods described by Hakki/Paoli and Cassidy. The residual reflectivity of the modal reflectivity design was lower than the plane wave design, although neither was as low as anticipated. This could be attributed to a potential thickness reduction due to shadowing of the laser facet by the 700 μm thick piece of silicon wafer used to clamp the laser in place during the deposition. The recommendation for future depositions is to ensure that the laser facet stands above any clamping surfaces such that shadowing is not able to take place.

An estimate was made of the effects of uncertainties in index and thickness on the spectral reflectivity profile of a single layer AR coating as deposited on a laser facet. The results indicate that films grown at the extremes of the deposition system's tolerances

should reach reflectivities below 10^{-4} at the design wavelength. However, given the discrepancies between the measured and theoretical AR coatings, it would be desirable to further optimize the ECR-CVD system, in order to facilitate growth of increasingly reproducible films in the future.

Finally, high reflectance coatings are also of interest. To demonstrate our capability to deposit high quality HR stacks, a four layer coating was deposited on a 980 nm laser. This coating had a broadband peak reflectivity of over 90% as measured on both the witness sample and the laser facet. Such a coating would be ideal as one of the mirrors in an external cavity design, particularly for a cavity utilizing a Bragg grating fiber.

6.4 Future Work

The work discussed in this thesis has set the stage for a long term, large scale research initiative to develop improved mode locked diode lasers. As such, it is worthwhile to conclude by discussing a potential long term "plan of attack" to move this project from the introductory stages to a state of maturity. Currently, no lasers have been mode locked, so the first step in this direction is to demonstrate mode locking of a diode laser in an external cavity.

Realistically, it will be necessary to mount the diode laser in an external cavity to actively mode lock it, and to make the measurements needed to verify that the laser is indeed mode locked. From my standpoint, the first steps in external cavity development

should achieve feedback using a single mirror, mounted to allow adjustable cavity length. There are two possible configurations for such a simple cavity. The first would consist of a 100% reflectivity mirror coupling light through a lens into the rear AR coated facet of a laser diode with an uncoated front facet, as shown in figure 6.1a. The second approach (figure 6.1b) would involve HR coating the rear facet of the diode laser and providing feedback via a partially reflecting mirror through the front facet of the laser. Eventually, more sophisticated cavities could be developed employing diffraction grating feedback to provide additional control of the spectral properties of the laser. Alternatively, a fiber grating could be used to replace the mirror in figure 6.1b to serve the dual purpose of providing feedback and fiber amplifier compatibility. Because the absorbing section of a split contact diode laser is effectively a photodiode, the amount of external cavity feedback can be optimized by maximizing the photocurrent detected by a small absorbing section.

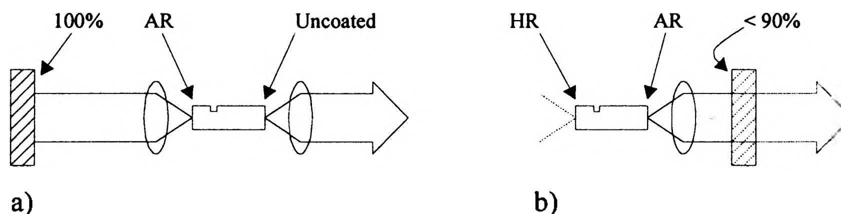

Figure 6.1: Two possible external cavity configurations.

Once a suitable external cavity system is functional, steps should be taken to achieve mode locking using the external cavity lasers. Passive mode locking may be achieved by adjusting the absorber section bias of a split contact laser with characteristics identified in chapter 4. Active mode locking will require the diode to be driven with an RF signal. An initial RF oscillator system has been developed which will provide up to

28 dBm of RF power into the lasers through a bias-T. The frequency of the oscillator is tunable over a range of 275 MHz to 560 MHz. Thus the applied RF can be tuned to match the round trip frequency of the external cavity. The current RF oscillator is therefore suitable for external cavity lengths ranging from 54 cm to 27 cm. Other tunable master oscillators may be purchased for the circuit to allow operation at higher frequencies and correspondingly shorter cavity lengths.

Finally, once active, passive, and hybrid mode locking have been successfully demonstrated and optimized, steps should be taken to achieve shorter pulses and high peak powers. Shorter pulses will be attainable by utilizing grating or fiber pulse compressors as discussed in chapter 2. Higher power pulses could be produced by using high power semiconductor laser amplifiers to amplify the master laser oscillator's output. If a fiber grating cavity is used, the amplification could be provided by a rare earth doped fiber amplifier. By introducing the amplification stage before the pulse compression, higher peak power pulses will be attainable by ensuring the peaks do not exceed the saturation energy of the amplifier.

References

[1] H. Kapteyn and M. Murnane, "Ultrashort light pulses: life in the fast lane," *Physics World*, pp. 31-35, January 1999.

[2] C. Spielmann, P. F. Curley, T. Brabec, and F. Krausz, "Ultrabroadband femtosecond lasers," *IEEE J. Quantum Electron.* **30**, pp. 1100-1114, 1994.

[3] T. Y. Fan and R. L. Byer, "Diode laser-pumped solid-state lasers," *IEEE J. Quantum Electron.* **24**, pp. 895-912, 1988.

[4] P. Vasil'ev, *Ultrafast Diode Lasers, Fundamentals and Applications*, Artech House Inc., Norwood, 1995.

[5] P. T. Ho, L. A. Glasser, E. P. Ippen, and H. A. Haus, "Picosecond pulse generation with a CW GaAlAs laser diode," *Appl. Phys. Lett.* **33**, pp. 241-242, 1978.

[6] D. J. Derickson, R. J. Helkey, A. Mar, J. R. Karin, J. G. Wasserbauer, and J. E. Bowers, "Short pulse generation using multisegment mode-locked semiconductor lasers," *IEEE J. Quantum Electron.* **28**, pp. 2186-2201, 1992.

[7] Y. Silberberg, P. W. Smith, D. J. Eilenberger, D. A. B. Miller, A. C. Gossard, and W. Wiegmann, "Passive mode locking of a semiconductor diode laser," *Opt. Lett.* **9**, pp. 507-509, 1984.

[8] J. Yu, M. Schell, M. Schulze, and D. Bimberg, "Fourier limited 1.6-ps pulses with variable repetition rate from 1 to 26 GHz by passive mode-locking of a

semiconductor laser in an external cavity," *IEEE Phot. Tech. Lett.* **7**, pp. 467-469, 1995.

[9] P. J. Delfyett, L. Florez, N. Stoffel, T. Gmitter, N. Andreadakis, G. Alphonse, and W. Ceislik, "200-fs optical pulse generation and intracavity pulse evolution in a hybrid mode-locked semiconductor diode-laser/amplifier system," *Opt. Lett.* **17**, pp. 670-672, 1992.

[10] P. J. Delfyett, L. T. Florez, N. Stoffel, T. Gmitter, N. C. Andreadakis, Y. Silberberg, J. P. Heritage, and G. A. Alphonse, "High-power ultrafast laser diodes," *IEEE J. Quantum Electron.* **28**, pp.2203-2219, 1992.

[11] A. Azouz, N. Stelmakh, P. Langlois, J. Lourtioz, and P. Gavrilovic, "Nonlinear chirp compensation in high-power broad-spectrum pulses from single-stripe mode-locked laser diodes," *IEEE J. Select. Topics in Quantum Elect.* **1**, pp. 577-582, 1995.

[12] R. Nagar, D. Abraham, N. Tessler, A. Fraenkel, G. Eisenstein, E. P. Ippen, U. Koren, and G. Raybon, "Frequency-modulation mode locking of a semiconductor laser," *Opt. Lett.* **16**, pp. 1750-1752, 1991.

[13] P. P. Vasil'ev, "Ultrashort pulse generation in diode lasers," *Optical and Quantum Electronics* **24**, pp. 801-824, 1992.

[14] A. Mar, D. Derickson, R. Helkey, J. Bowers, R. Huang, and D. Wolf, "Actively mode-locked external-cavity semiconductor lasers with transform-limited single-pulse output," *Opt. Lett.* **17**, pp. 868-870, 1992.

[15] J. E. Bowers, P. A. Morton, A. Mar, and S. W. Corzine, "Actively mode-locked semiconductor lasers," *IEEE J. Quantum Electron.* **25**, pp.1426-1439, 1989.

[16] L. A. Coldren and S. W. Corzine, *Diode Lasers and Photonic Integrated Circuits*, John Wiley & Sons Inc., New York, 1995.

[17] D. S. Chemla, D. A. B. Miller, P. W. Smith, A. C. Gossard, W. Wiegmann, "Room temperature excitonic nonlinear absorption and refraction in GaAs/AlGaAs multiple quantum well structures," *IEEE J. Quantum Electron.* **QE-20**, pp 265-275, 1984.

[18] E. P. Ippen, D. J. Eilenberger, and R. W. Dixon, "Picosecond pulse generation by passive modelocking of diode lasers," *Appl. Phys. Lett.* **37**, pp. 267-269, 1980.

[19] J. P. van der Ziel, W. T. Tsang, R. A. Logan, R. M. Mikulyak, and W. M. Augustyniak, "Subpicosecond pulses from passively modelocked GaAs buried optical guide semiconductor laser," *Appl. Phys. Lett.* **39**, pp. 525-527, 1981.

[20] D. J. Derickson, R. J. Helkey, A. Mar, J. R. Karin, J. E. Bowers, and R. L. Thornton, "Suppression of multiple pulse formation in external-cavity mode-locked semiconductor lasers using intrawaveguide saturable absorbers," *IEEE Phot. Tech. Lett.* **4**, pp. 333-335, 1992.

[21] D. Burns, A. Finch, W. Sleat, and W. Sibbett, "Noise characterization of a mode-locked InGaAsP semiconductor diode laser," *IEEE J. Quantum Electron.* **26**, pp. 1860-1863, 1990.

[22] A. G. Weber, M. Schell, G. Fischbeck, and D. Bimberg, "Generation of single femosecond pulses by hybrid mode locking of a semiconductor laser," *IEEE J. Quantum Electron.* **28**, pp.2220-2229, 1992.

[23] J. Yu, M. Schell, M. Schulze, and D. Bimberg, "Generation of 290 fs pulses at 1.3 mm by hybrid mode-locking of a semiconductor laser and optimization of the time-bandwidth product," *Appl. Phys. Lett.* **65**, pp. 2395-2397, 1994.

[24] P. A. Morton, V. Mizrahi, T. Tanbun-Ek, R. A. Logan, P. Lemaire, T. Erdogan, P. F. Sciortino Jr., A. M. Sergent, and K. W. Wecht, "High-power mode-locked hybrid pulse source using two-section laser diodes," *Opt. Lett.* **19**, pp. 725-727, 1994.

[25] E. B. Treacy, "Optical pulse compression with diffraction gratings," *IEEE J. Quantum Electron.* **QE-5**, pp. 454-458, 1969.

[26] M. Kuznetsov, J. M. Wiesenfeld, and L. R. Radzihovsky, "Compression of picosecond pulses from diode lasers using a modified grating-pair compressor," *Opt. Lett.* **15**, pp. 180-182, 1990.

[27] K. A. Ahmed, B. J. Eggleton, H. Liu, P. A. Krug, and F. Ouellette, "Simultaneous mode selection and pulse compression of gain-switched pulses from a Fabry-Perot laser using a 40-mm chirped optical fiber grating," *IEEE Phot. Tech. Lett.* **7**, pp. 158-160, 1995.

[28] A. Galvanauskas, P. A. Krug, and D. Harter, "Nanosecond-to-picosecond pulse compression with fibre gratings in a compact fiber-based chirped-pulse-amplification system," *Opt. Lett.* **21**, pp. 1049-1051, 1996.

[29] A. Galvanauskas, P. Blixt, and J. A. Tellefsen Jr., "Generation of femtosecond optical pulses with nanojoule energy from a diode laser and fiber based system," *Appl. Phys. Lett.* **63**, pp. 1742-1744, 1993.

[30] M. R. Gokhale, J. C. Dries, P. Studenkov, D. Z. Garbuzov, and S. R. Forrest, "Low loss, low-threshold 0.98μm wavelength InGaAsP/InGaP/GaAs broadened waveguide lasers grown by GSMBE," *1997 IEEE International Conference on Indium Phosphide and Related Materials*, pp. 296-299, 1997.

[31] G. Zhang, J. Näppi, K. Vänttinen, H. Asonen, and M. Pessa, "Low threshold current InGaAs/GaAs/GaInP lasers grown by gas-source molecular beam epitaxy," *Appl. Phys. Lett.* **61**, pp. 96-98, 1992.

[32] H. Asonen, A. Ovtchinnikov, G. Zhang, J. Näppi, P. Savolainen, and M. Pessa, "Aluminum-free 980-nm GaInAs/GaInAsP/GaInP pump lasers," *IEEE J. Quantum Elect.* **30**, pp. 415-423, 1994.

[33] L. J. Mawst, A. Bhattacharya, J. Lopez, D. Botez, D. Z. Garbuzov, L. DeMarco, J. C. Connolly, M. Jansen, F. Fang, and R. F. Nabiev, "8W continuous wave front-facet power from broad-waveguide Al-free 980 nm diode lasers," *Appl. Phys. Lett.* **69**, pp. 1532-1534, 1996.

[34] T. Panarello, "Growth Optimization and Fabrication of 980 nm InGaAs/GaAs/InGaP Lasers," M.Eng. Thesis, McMaster University, 1997.

[35] G. Zhang, J. Näppi, and M. Pessa, "GaAs/GaInAsP quantum well lasers grown by gas-source molecular beam epitaxy," *Appl. Phys. Lett.* **64**, pp. 1009-1011, 1994.

[36] W. E. Plano, J. S. Major Jr., and D. F. Welch, "High power 875 nm Al-free laser diodes," *IEEE Phot. Tech. Lett.* **6**, pp. 465-467, 1994.

[37] D. Z. Garbuzov, N. Y. Antonishkis, A. D. Bondarev, A. B. Gulakov, S. N. Zhigulin, N. I. Katsavets, A. V. Kochergin, and E. V. Rafailov, "High-power 0.8μm InGaAsP-GaAs SCH SQW lasers," *IEEE J. Quantum Elect.* **27**, pp. 1531-1535, 1991.

[38] S. L. Yellen, A. H. Shepard, C. M. Harding, J. A. Baumann, R. G. Walters, D. Z. Garbuzov, V. Pjataev, V. Kochergin, P. S. Zory, "Dark-line-resistant, aluminum-free diode laser at 0.8 μm," *IEEE Phot. Tech. Lett.* **4**, pp. 1328-1330, 1992.

[39] G. Zhang, J. Näppi, H. Asonen, and M. Pessa, "Tensile-strained GaAsP/GaInAsP/GaInP quantum well lasers," *IEEE Phot. Tech. Lett.* **6**, pp. 1-3, 1994.

[40] H. J. Yi, J. Diaz, L. J. Wang, I. Eliashevich, S. Kim, R. Williams, M. Erdtmann, X. He, E. Kolev, and M. Razeghi, "Optimized structure for InGaAsP/GaAs 808 nm high power lasers," *Appl. Phys. Lett.* **66**, pp. 3251-3253, 1995.

[41] I. Eliashevich, J. Diaz, H. Yi, L. Wang, and M. Razeghi, "Reliability of aluminum-free 808 nm high-power laser diodes with uncoated mirrors," *Appl. Phys. Lett.* **66**, pp. 3087-3089, 1995.

[42] K. J. Vahala and M. A. Newkirk, "Parasitic-free modulation of semiconductor lasers," *IEEE J. Quantum Elect.* **25**, pp. 1393-1398, 1989.

[43] P. S. Zory, Jr., *Quantum Well Lasers*, Academic Press Inc., San Diego, 1993.

[44] S. G. Wallace, "Design of an InGaAsP/InP Semiconductor Laser," unpublished.

[45] S. L. Chuang, Physics of Optoelectronic Devices, John Wiley & Sons, Inc., New York, 1995.

[46] X. Zeng and A. Naqwi, "Far-field distribution of double-heterostructure diode laser beams," *Appl. Opt.* **32**, pp. 4491-4494, 1993.

[47] H. Kawaguchi and T. Kawakami, "Transverse-mode control in an injection laser by a strip-loaded waveguide," *IEEE J. Quantum Elect.* **QE-13**, pp. 556-560, 1977.

[48] G. P. Agrawal, *Semiconductor Lasers, Second Edition*, van Nostrand Reinhold, New York, 1993.

[49] H. Burkhard, H. W. Dinges, and E. Kuphal, "Optical properties of $In_{1-x}G_xP_{1-y}As_y$, InP, GaAs, and GaP determined by ellipsometry," *J. Appl. Phys.* **53**, pp. 655-662, 1982.

[50] S. Adachi, "Refractive indices of III-IV compounds: key properties of InGaAsP relevant to device design," *J. Appl. Phys.* **53**, pp. 5863-5869, 1982.

[51] M. Amiotti and G. Landgren, "Ellipsometric determination of thickness and refractive index at 1.3, 1.55, and 1.7mm for $In_{(1-x)}Ga_xAs_yP_{(1-y)}$ films on InP," *J. Appl. Phys.* **73**, pp. 2965-2971, 1993.

[52] M. Pessa, and H. Asonen, "Recent advances in compound semiconductor technology," *Opt. Eng.* **34**, pp. 2521-2526, 1995.

[53] M. Pessa, K. Tappura, and A. Ovtchinnikov, "GaInAsP gas-source MBE technology," *Thin Solid Films* **267**, pp. 99-105, 1995.

[54] D. E. Aspnes and A. A. Studna, "Dielectric functions and optical parameters of Si, Ge, GaP, GaAs, GaSb, InP, InAs, and InSb from 1.5 to 6.0 eV," *Physical Review B* **27**, pp. 985-1009, 1983.

[55] G. Zhang, M. Pessa, K. Hjelt, H. Collan, and T. Tuomi, "Gas-source molecular beam epitaxy of lattice-matched $Ga_xIn_{1-x}As_yP_{1-y}$ on GaAs over the entire composition range," *J. Crystal Growth* **150**, pp. 607-611, 1995.

[56] S. Nagy, Private communication.

[57] R. R. LaPierre, T. Okada, B. J. Robinson, D. A. Thompson, and G. C. Weatherly, "Spinodal-like decomposition of InGaAsP/(100)InP grown by gas source molecular beam epitaxy," *J. Crystal Growth* **155**, pp. 1-15, 1995.

[58] H. S. Gingrich, D. R. Chumney, S.-Z. Sun, S. D. Hersee, L. F. Lester, S. R. J. Brueck, "Broadly tunable external cavity laser diodes with staggered thickness multiple quantum wells," *IEEE Phot. Tech. Lett.* **9**, pp.155-157, 1997.

[59] M. J. Hamp, D. T. Cassidy, B. J. Robinson, Q. C. Zhao, D. A. Thompson, and M. Davies, "Effect of barrier height on the uneven carrier distribution in asymmetric multiple-quantum-well InGaAsP lasers," *IEEE Phot. Tech. Lett.* **10**, pp.1380-1382, 1998.

[60] L. Goldberg, D. Mehuys, and D. Welch, "High power mode-locked compound laser using a tapered semiconductor amplifier," *IEEE Phot. Tech. Lett.* **6**, pp.1070-1072, 1994.

[61] D. Mehuys, L. Goldberg, and D. F. Welch, "5.25-W CW near-diffraction-limited tapered-stripe semiconductor optical amplifier," *IEEE Phot. Tech. Lett.* **5**, pp. 1179-1182, 1993.

[62] A. Mar, R. Helkey, W. X. Zou, D. B. Young, and J. E. Bowers, "High-power mode-locked semiconductor lasers using flared waveguides," *Appl. Phys. Lett.* **66**, pp.3558-3560, 1995.

[63] K. Y. Lau, C. Harder, and A. Yariv, "Interaction of a bistable injection laser with an external optical cavity," *Appl. Phys. Lett.* **40**, pp. 369-371, 1982.

[64] K. Y. Lau and A. Yariv, "Bistability and pulsations in semiconductor lasers with inhomogeneous current injection," *IEEE J. Quantum Electron.* **QE-18**, pp.1351-1360, 1982.

[65] J. Swoger, "On Non-Uniform Pumping Effects in Semiconductor Lasers," Ph.D. Thesis, McMaster University, 1997.

[66] P. Phelan et. al. "Comparison of self-pulsation in multisection lasers with distributed feedback and intracavity saturable absorbers," *IEE Proc. Optoelectron.* **141**, pp. 114-118, 1994.

[67] C. Harder, K. Y. Lau, and A. Yariv, "Bistability and negative resistance in semiconductor lasers," *Appl. Phys. Lett.* **40**, pp. 124-126, 1982.

[68] C. Harder, J. S. Smith, Kam Y. Lau, and A. Yariv, "Passive mode locking of buried heterostructure lasers with nonuniform current injection," *Appl. Phys. Lett.* **42**, pp. 772-774, 1983.

[69] K. Y. Lau and J. Paslaski, "Condition for short pulse generation in ultrahigh frequency mode-locking of semiconductor lasers," *IEEE Trans. Phot. Tech. Lett.* **3**, pp. 974-976, 1991.

[70] H. A. Haus, "Theory of mode locking with a slow saturable absorber," *IEEE J. Quantum Elect.* **QE-11**, pp. 736-746, 1975.

[71] H. A. Haus, "Modelocking of semiconductor laser diodes," *Jap. J. of Appl. Phys.* **20**, pp. 1007-1020, 1981.

[72] J. Buus, M. C. Farries, and D. J. Robbins, "Reflectivity of coated and tilted semiconductor facets," *IEEE J. Quantum Elect.* **27**, pp. 1837-1842, 1991.

[73] M. G. Boudreau, S. G. Wallace, G. Balcaitis, S. Murugkar, H. K. Haugen, and P. Mascher, "Application of in-situ ellipsometry in the fabrication of thin film optical coatings on semiconductors," *Appl. Opt.* (submitted).

[74] K. Wakita and S. Matsuo, "Small surface damage facet coating on InGaAsP/InP laser by ECR plasma deposition," *Jap. J. Appl. Phys.* **23**, pp. L556-L558, 1984.

[75] S. Dzioba and R. Rousina, "Dielectric thin film deposition by electron cyclotron resonance plasma chemical vapor deposition for optoelectronics," *J. Vac. Sci. Technol. B* **12**, pp. 433-440, 1994.

[76] M. Boudreau, M. Boumerzoug, P. Mascher, and P. E. Jessop, "Electron cyclotron resonance chemical vapor deposition of silicon oxynitrides using tris(dimethylamino)silane," *Appl. Phys. Lett.* **63**, pp. 3014-3016, 1993.

[77] Ch. Wettlaufer, (unpublished).

[78] D. M. Braun and R. L. Jungerman, "Broadband multilayer antireflection coating for semiconductor laser facets," *Opt. Lett.* **20**, pp.1154-1156, 1995.

[79] J. A. Dobrowolski, A. V. Tikhonravov, M. K. Trubetskov, B. T. Sullivan, and P. G. Verly, "Optimal single-band normal-incidence antireflection coatings," *Appl. Opt.* **35**, pp. 644-658, 1996.

[80] C. Vassallo, "Reflectivity of multidielectric coatings deposited on the end facet of a weakly guiding dielectric slab waveguide," *J. Opt. Soc. Am. A* **5**, pp. 1918-1928, 1988.

[81] C. Vassallo, "Rigorous and approximate calculations of antireflection layer parameters for travelling-wave diode laser amplifiers," *Elect. Lett.* **21**, pp. 333-334, 1985.

[82] M. G. Boudreau, "Optical Coatings for Improved Semiconductor Diode Laser Performance," Ph.D. Thesis, McMaster University, 1997.

[83] D. T. Cassidy, "Technique for measurement of the gain spectra of semiconductor diode lasers," *J. Appl. Phys.* **56**, pp. 3096-3099 1984.

[84] B. W. Hakki and T. L. Paoli, "CW degredation at 300°K of GaAs double-heterostructure junction lasers. II. Electronic gain," *J. Appl. Phys.* **44**, pp. 4113-4119, 1973.

[85] B. W. Hakki and T. L. Paoli, "Gain spectra in GaAs double-heterostructure injection lasers," *J. Appl. Phys.* **46**, pp. 1299-1306, 1975.

[86] M. P. Kesler, and C. Harder, "Gain and index measurements in GaAlAs quantum well lasers," *IEEE Phot. Tech. Lett.* **2**, pp. 464-466, 1990.

[87] D. J. Gallant, M. L. Tilton, D. J. Brossert, J. D. Barrie, and G. C. Dente, "Optimized single-layer antireflection coatings for semiconductor lasers," *IEEE Phot. Tech. Lett.* **9**, pp. 300-302, 1997.

[88] T. Saitoh, T. Mukai, and O. Mikami, "Theoretical analysis and fabrication of antireflection coating of laser-diode facets," *J. Lightwave Tech.* **LT-3**, pp.288-293, 1985.